

Exploring Neutrino Phenomenology and $0\nu\beta\beta$ Decay in a Left-Right Asymmetric Model with A_4 Modular Symmetry

Bhabana Kumar^{1,*} and Mrinal Kumar Das^{1,†}

¹*Department of Physics, Tezpur University, Tezpur 784028, India*

Abstract

In this study, we explore the application of the $\Gamma(3)$ modular group, which is isomorphic to the A_4 symmetric group, in developing a model for neutrino mass. We construct a left-right asymmetric model using modular symmetry, which offers the advantage of eliminating the need for additional particles known as "flavons." The Yukawa coupling term is expressed in terms of modular forms denoted as Y_1 , Y_2 , and Y_3 . To effectively implement the extended see-saw process in this model, we introduce one fermion singlet for each generation. We compute the effective mass and the associated half-life of $0\nu\beta\beta$ by accounting for both standard and non-standard contributions. Additionally, our study investigates the non-unitary effects and CP-violation arising from non-unitarity in this context. The model predicts values for the sum of neutrino masses and neutrino oscillation parameters are constraints with experiments. Furthermore, it yields satisfactory results in calculating the effective mass and half-life of $0\nu\beta\beta$ decay. These findings underscore the viability and utility of employing modular symmetry in neutrino mass model construction.

arXiv:2405.10586v1 [hep-ph] 17 May 2024

* bhabana12@tezu.ernet.in

† mkdas@tezu.ernet.in

I. INTRODUCTION

One of the most recognized and thoroughly tested particle physics models to date is the standard model (SM). In addition to explaining interactions between all of the known fundamental particles, SM also describes their properties, such as mass, charge, spin, and so forth. Despite being successful, SM is not without limitations. One significant drawback is its inability to account for the tiny neutrino masses. Except for the neutrino, every fermion in the context of SM is massive, and the Higgs mechanism gives those fermions their mass. The Higgs mechanism requires both the left and right-handed counter particles to couple with the Higgs field for a particle to gain mass. However, due to the lack of right-handed counter particles of neutrinos, it is not possible to incorporate massive neutrinos within the framework of SM. The idea of a massless neutrino is completely denied by the discovery of neutrino oscillation. Experiments like Superkamiokande [1] and SNO [2–4] have provided strong evidence for neutrino oscillation, a phenomenon that is not possible if the neutrino is massless. To learn more about neutrinos, several experiments, including MINOS [5], Daya-Bay [6], TK2 [7], RENO [8], and others, have been carried out, and all those experiments have suggested non-zero and non-degenerate neutrino masses. Neutrino oscillation experiments have played a crucial role in refining our knowledge of neutrinos and providing insights into their properties. Scientists have been able to determine the mass squared differences and mixing angles associated with neutrinos. While substantial progress has been made in determining the oscillation parameter, there is still much we do not know definitively about neutrinos. The Planck experiment recently provided an approximate upper bound on the sum of the neutrino masses, which is equal to $\sum m_\nu = 0.11$ eV [9]. However, the exact masses of neutrino and their mass hierarchy [10, 11] remain unclear. Additionally, the nature of neutrinos, whether they are Dirac or Majorana particles [12, 13], is still a subject of ongoing study.

The limitations of the SM extend beyond neutrino masses. It fails to explain phenomena such as CP violation in weak interactions, lepton flavor violation, the baryon asymmetry of the universe, dark matter, and dark energy. To address these shortcomings, we need to go beyond the standard model and explore extensions that involve the addition of new fermion or scalar particles. The seesaw mechanism is a prominent extension that offers explanations to the tiny neutrino mass problem. There are different types of seesaw mechanisms, such as Type I [14–16], Type II [17–19], and Type III [20]. In these models, the SM is extended by incorporating a right-handed neutrino, an $SU(2)_L$ scalar triplet, or an $SU(2)_L$ triplet fermion, respectively, to generate small but non-zero neutrino masses.

Another beyond SM framework is the Left-Right symmetric model (LRSM) [21–24], which extends the SM by introducing additional gauge symmetries. The gauge group of the LRSM is $SU(3)_C \times SU(2)_L \times SU(2)_R \times U(1)_{B-L} \times D(G_{221D})$. This model has gained significant attention in the literature due to its success in explaining the tiny neutrino masses observed experimentally as well as addressing other

drawbacks of the SM. Even though the model is very successful in many aspects, ambiguity arises when one wants to incorporate the LRSM within the Grand Unified Theory (GUT). To embed LRSM within GUT like $S_0(10)$, requires the parity breaking scale to be very high, only then one will get the observed value of $\sin^2 \theta_W$ [25], but in LRSM both the D-parity and $SU(2)_R$ gauge groups break at the same energy scale, which implies that all the phenomena involving right-handed current will get highly suppressed under this condition. However, an alternative approach to the LRSM is the left-right asymmetric model [26, 27], where the D-parity is decoupled from the $SU(2)_R$ gauge group at a very high energy scale. This decoupling results in different gauge coupling values for the $SU(2)_L$ and $SU(2)_R$ gauge groups, leading to an asymmetry in the model. In this left-right asymmetric model, the gauge coupling value of $SU(2)_L$ is not equal to the gauge coupling value of $SU(2)_R$, that is, $g_l \neq g_r$. This alternative approach is intriguing because the different gauge coupling values can either suppress or enhance various low-energy phenomena, offering unique predictions.

For many years discrete symmetry group like A_4 , S_4 , S_3 have been used for model building purpose in the lepton sector [28–31]. But one of the main disadvantage is the requirement of "flavon" to spontaneously break such symmetry and vacuum expectation value (V.E.V) of such field can significantly effect the physical prediction of the model. In recent years, the application of modular symmetry in particle physics has received significant attention due to its ability to explain the patterns and hierarchies observed in the masses and mixing of fermions also modular symmetry gained its popularity because one can construct a model without using any "flavon" or with the minimal number of "flavon" since in modular symmetry modulus τ is responsible for breaking the flavor symmetry [32, 33]. Many research groups have been working on model building by using modular group like $\Gamma(3)$ [34–39], $\Gamma(4)$, [40, 41] $\Gamma(5)$ [42] etc. In our current work, we have focused on studying neutrino masses and mixing within the left-right asymmetric model. We have studied neutrinoless double beta ($0\nu\beta\beta$) decay within this frame work. To realize this asymmetric model, we have employed the $\Gamma(3)$ modular group, which is isomorphic to the A_4 discrete symmetry group. By utilizing this mathematical framework, we have derived mass matrices that govern the neutrino sector of the model and implemented those matrices to calculate and study neutrino masses, effective neutrino mass, and half-life of $0\nu\beta\beta$ decay.

The overall structure of the paper is as follows:: In section II, we have given a brief introduction to the left-right asymmetric model, in section III, we have given an overview of modular symmetry; in section IV, we have thoroughly discussed the model; in section V, we have given a overview about extended inverse seesaw mechanism and in VI, we have discussed the unitary violation in the lepton sector. In Section VII, we have concisely discussed the contribution to $0\nu\beta\beta$ decay, and a rigorous discussion about the numerical analysis and results of our study is given in Section VIII. Finally, in Section IX, we have concluded our study.

II. LEFT-RIGHT ASYMMETRIC MODEL

The initial proposal of the left-right asymmetry model was put forth by Chang, Mohapatra, and Parida in their publication [43]. An alternate method has been proposed to decouple D-parity from the $SU(2)_R$ gauge group at high energy scales while preserving the original gauge symmetry intact [26, 27]. The decoupling of D-parity from the $SU(2)_R$ gauge group occurs initially when the odd parity singlet scalar field η , has a vacuum expectation value at an energy scale denoted as M_P . The outcome is an asymmetrical left-right model in which the gauge coupling of $SU(2)_L$ and $SU(2)_R$ becomes unequal, i.e. $g_l \neq g_r$. The entire symmetry breaking steps can be illustrated as follows.

$$\begin{aligned}
& SU(2)_L \times SU(2)_R \times U(1)_{B-L} \times SU(3)_C \times D \\
& \quad \downarrow \quad \sigma \\
& SU(2)_L \times SU(2)_R \times U(1)_{B-L} \times SU(3)_C \\
& \quad \downarrow \Sigma \\
& SU(2)_L \times U(1)_R \times U(1)_{B-L} \times SU(3)_C \\
& \quad \downarrow \Delta_R \\
& SU(2)_L \times U(1)_Y \times SU(3)_C \\
& \quad \downarrow \quad \Phi \\
& U(1)_{em} \times SU(3)_C.
\end{aligned}$$

After the spontaneous breaking of D-parity, the asymmetric gauge group undergoes two possible paths. The first path occurs when the Higgs triplet Δ_R gains a non-zero vacuum expectation value, leading to the breakdown of the left-right asymmetric model into SM gauge group. Subsequently, SM gauge group further breaks down to $U(1)_{em}$ when both the left-handed Higgs triplet and the bidoublet acquire non-zero V.E.V.

On the other hand, in the alternative path, the gauge group $SU(2)_R$ initially breaks down to $U(1)_R$ when a heavier scalar triplet, $\Sigma(1, 3, 0)$, carrying $B - L = 0$, obtains a non-zero V.E.V. This step of symmetry breaking leads to the generation of massive W_R^\pm gauge bosons. Finally, in the last step, the intermediate gauge group $U(1)_R \times U(1)_{B-L}$ breaks down to SM gauge group when either a doublet, a triplet, or both the doublet and triplet gain non-zero V.E.V [44]. During this step, the right-handed neutral gauge boson Z_R^0 obtains its mass. The minimal particle content of the model and their charge assignment under the gauge group G_{221} are given below

$$Q_L = \begin{pmatrix} u_L \\ d_L \end{pmatrix}, \quad Q_R = \begin{pmatrix} u_R \\ d_R \end{pmatrix}, \quad \Psi_L = \begin{pmatrix} \nu_L \\ l_L \end{pmatrix}, \quad \Psi_R = \begin{pmatrix} \nu_R \\ l_R \end{pmatrix}$$

$$Q_L : (1/2, 0, 1/3) \quad Q_R : (0, 1/2, 1/3) \quad \Psi_L : (1/2, 0, -1) \quad \Psi_R : (0, 1/2, -2)$$

and the required Higgs multiplets are

$$\phi = \begin{pmatrix} \phi_1^0 & \phi_1^+ \\ \phi_2^- & \phi_2^0 \end{pmatrix}, \quad \Delta_{L,R} = \begin{pmatrix} \frac{\delta_{L,R}^+}{\sqrt{2}} & \delta_{L,R}^{++} \\ \delta_{L,R}^0 & -\frac{\delta_{L,R}^+}{\sqrt{2}} \end{pmatrix}$$

$$\sigma(1, 1, 0), \quad \Phi(2, 2, 0), \quad \Delta_L(3, 1, +2) + \Delta_R(1, 3, +2) .$$

We can write the individual potential term as follows [43]

$$\begin{aligned} V_\Delta &= \mu_\Delta^2 [Tr(\Delta_L^\dagger \Delta_L) + Tr(\Delta_R^\dagger \Delta_R)] \\ V_\eta &= -\mu_\eta^2 \eta^2 + \lambda \eta^4 \\ V_{\eta\Delta} &= M\eta [Tr(\Delta_L^\dagger \Delta_L) - Tr(\Delta_R^\dagger \Delta_R)] + \lambda_1 \eta^2 [Tr(\Delta_L^\dagger \Delta_L) + Tr(\Delta_R^\dagger \Delta_R)] \\ V_{\eta\Phi} &= \lambda_2 \eta^2 Tr(\phi^\dagger \phi) + \lambda_3 \eta^2 (det\Phi + det\tilde{\Phi}) \\ V_{\Delta\Phi} &= \lambda_5 [Tr(\tilde{\Phi})\Delta_R\Phi^\dagger\Delta_L^\dagger + Tr(\tilde{\Phi}^\dagger\Delta_L\Phi\Delta_R^\dagger)] \\ V_\Phi &= \mu_1^2 Tr(\Phi^\dagger\Phi) + \mu_2^2 [Tr(\tilde{\Phi}^\dagger\Phi) + Tr(\Phi^\dagger\tilde{\Phi})] \end{aligned}$$

After the spontaneous symmetry breaking we can choose the V.E.V of $\Delta_{L,R}$ and ϕ as follows

$$\langle \Delta_{L,R} \rangle = \frac{1}{\sqrt{2}} \begin{pmatrix} 0 & 0 \\ \nu_{L,R} & 0 \end{pmatrix}, \quad \langle \Phi \rangle = \begin{pmatrix} k & 0 \\ 0 & \exp(i\phi)k' \end{pmatrix}$$

and the D-parity is broken by $\langle \eta \rangle = \frac{\mu}{\sqrt{2}\lambda}$, which then makes the Δ_L and Δ_R mass terms asymmetric.

III. MODULAR GROUP

The modular group $SL(2, Z) = \Gamma$ is defined as a group of 2×2 matrices with positive or negative integer element and determinant equal to 1 and it represents the symmetry of a torus [45, 46]. It is infinite group and generated by two generator of the group S and T .

$$\Gamma = \left\{ \begin{pmatrix} a & b \\ c & d \end{pmatrix} \mid a, b, c, d \in \mathbb{Z}, ad - bc = 1 \right\} . \quad (3.1)$$

The generator of the group satisfy the conditions:

$$S^2 = 1 \quad \text{and} \quad (ST)^3 = 1$$

and they can be represented by 2×2 matrices

$$S = \begin{pmatrix} 0 & 1 \\ -1 & 0 \end{pmatrix}, \quad T = \begin{pmatrix} 1 & 1 \\ 0 & 1 \end{pmatrix} .$$

A two dimensional space is obtained, when the torus is cut open and this two dimensional space can be viewed as an Argand plane and modulus τ is the lattice vector of that Argand plan. The transformation of modulus τ [47] of the modular group on the upper half of the complex plan is given bellow

$$\gamma : \tau \rightarrow \gamma(\tau) = \frac{(a\tau + b)}{(c\tau + d)}$$

the transformation of τ is same for both γ and $-\gamma$ and we can define a group $\bar{\Gamma} = PSL(2, Z)$, which is a projective special linear group. Also the modular group has infinite number of normal subgroups, which is the principal congruence subgroup of level N and can be define as

$$\Gamma(N) = \left\{ \begin{pmatrix} a & b \\ c & d \end{pmatrix} \in SL(2, Z), \begin{pmatrix} a & b \\ c & d \end{pmatrix} = \begin{pmatrix} 1 & 0 \\ 0 & 1 \end{pmatrix} \pmod{N} \right\}, \quad (3.2)$$

and for $N > 2$, $\bar{\Gamma}(N) = \Gamma_N$. In model building purpose it is efficient to use finite group. Usually a modular group is an infinite group but we can obtain a finite modular group for $N > 2$, if we consider the quotient group $\Gamma(N) = PSL(2, Z)/\bar{\Gamma}(N)$ and those modular group are isomorphic to non-abelian discrete groups. The quantity of Yukawa couplings expressed in terms of modular forms is dependent on the level and weight of the modular form when modular symmetry is utilized. Table I presented below provides information regarding the number of modular forms linked to a modular form of level N and weight $2k$, as well as the corresponding non-abelian discrete symmetry group to which it exhibits isomorphism [48]. To construct the present model we have used $\Gamma(3)$ modular group of weight two,

N	2	3	4	5	6	7
g	0	0	0	0	1	3
$d_{2k}(\Gamma N)$	$k + 1$	$2k + 1$	$4k + 1$	$10k + 1$	$12k$	$28k - 2$
μ_N	6	12	24	60	71	168
Γ_N	S_3	A_4	S_4	A_5		

TABLE I: Properties of modular group

which is a finite modular group and isomorphic to A_4 group. A_4 group is a non-abelian discrete group and have total four irreducible representation among which three are one dimensional and one is three dimensional. A brief introduction about the A_4 group is given in the Appendix **A**. As mention in the Table I, a $\Gamma(3)$ group of weight 2 have total three modular forms and those modular forms are corresponding to the three Yukawa coupling of the model. The q -expansion of the modular forms are given in the equation 3.3

$$\begin{aligned} Y_1(\tau) &= 1 + 12q + 36q^2 + 12q^3 + \dots \\ Y_2(\tau) &= -6q^{1/3}(1 + 7q + 8q^2 + \dots) \\ Y_3(\tau) &= -18q^{2/3}(1 + 2q + 5q^2 + \dots) \end{aligned} \quad (3.3)$$

where $q = e^{i2\pi\tau}$.

IV. THE MODEL

To implement $\Gamma(3)$ modular group, we have considered the intermediate asymmetric gauge group $SU(2)_L \times U(1)_R \times U(1)_{B-L} \times SU(3)_C$ and have used scalar triplet $(\Delta_{L,R})$ and doublet $(\chi_{L,R})$ to break the intermediate asymmetric group to SM gauge group. We have considered an extra sterile fermion per generation to generate the light neutrino mass via extended inverse seesaw mechanism [49–51]. The Yukawa Lagrangian term associated with the model is given in the equation 4.1

$$\mathcal{L} = \mathcal{L}_l + \mathcal{L}_D + \mathcal{L}_M + \mathcal{L}_{N-S} + \mathcal{L}_S + h.c. \quad . \quad (4.1)$$

Where \mathcal{L}_l is the Yukawa Lagrangian term for the charged lepton, \mathcal{L}_D is the Dirac Yukawa Lagrangian term for the neutral lepton, \mathcal{L}_M and \mathcal{L}_{N-S} are the majorana and neutrino-sterile (N-S) mixing term respectively and finally \mathcal{L}_S is the self coupling term for the sterile fermion. As we have considered the modular $\Gamma(3)$ group of weight two, we have total three modular forms and those modular forms are associated with the three Yukawa coupling of our model which is represented as (Y_1, Y_2, Y_3) . In Table II we have provided the charge assignments and modular weight for the particle contents of the model.

Field	Ψ_L	N_R	Ψ_R	S	Φ	Δ_R	χ_R
$SU(2)_L$	2	1	1	1	2	1	1
$U(1)_R$	0	$\frac{1}{2}$	$-\frac{1}{2}$	0	$-\frac{1}{2}$	1	$\frac{1}{2}$
$U(1)_{B-L}$	-1	-1	-1	1	0	2	-1
A_4	3	3	1, 1'', 1'	3	1	1	1
k_I	0	0	0	0	-2	-2	0

TABLE II: Charge assignment for the particle content of the model

The Yukawa coupling $Y = (Y_1, Y_2, Y_3)$ are represented as modular form of weight 3

	Modular form (Y)
A_4	3
k_I	2

TABLE III: Charge assignment and modular weight for Yukawa coupling

The charge assignment under $U(1)_R$ corresponds to the third or z-components of isospin i.e, T_{3R} of $SU(2)_R$ and the equation $Q = T_{3L} + T_{3R} + \frac{B-L}{2}$ is also valid for the gauge group G_{2113} . To make the

model consistence under $\Gamma(3)$ modular group, charge assignment under A_4 group is done in such a way so that each term of the Lagrangian is a trivial singlet under A_4 group and also the modular weight are given to the particle contents in such a way so that sum of the modular weight for each term of the Lagrangian is zero.

A. Dirac mass term for charge lepton

The lepton doublets Ψ_L transform as triplets under the A_4 group and the right handed charged leptons Ψ_R i.e. (e_R, μ_R, τ_R) transform as $(1, 1'', 1')$ under the A_4 group and on the other hand, the Higgs bidoublet transforms as a trivial singlet under the A_4 group. The A_4 invariant Yukawa Lagrangian term for the charged lepton sector is given in the equation (4.2)

$$\mathcal{L}_l = \bar{\Psi}_{R_1} \Phi(Y\Psi_L)_1 + \bar{\Psi}_{R_{1''}} \Phi(Y\Psi_L)_{1'} + \bar{\Psi}_{R_{1'}} \phi(Y\Psi_L)_{1''} \quad (4.2)$$

after the spontaneous symmetry breaking of the Lagrangian term given in equation (4.2), we obtain the Dirac mass matrix for the charged lepton sector, which is given in the equation (4.3).

$$M_l = v \begin{pmatrix} \alpha_1 & 0 & 0 \\ 0 & \alpha_2 & 0 \\ 0 & 0 & \alpha_3 \end{pmatrix} \cdot \begin{pmatrix} Y_1 & Y_3 & Y_2 \\ Y_2 & Y_1 & Y_3 \\ Y_3 & Y_2 & Y_1 \end{pmatrix} . \quad (4.3)$$

Where $(\alpha_1, \alpha_2, \alpha_3)$ are the free parameters of the model, we can adjust their values to get the desired charged lepton mass matrix and v is the V.E.V of the Higgs bidoublet Φ . We can make the charged lepton mass matrix diagonal by considering (Y_1, Y_2, Y_3) as $(1, 0, 0)$.

B. Dirac mass term for neutrino

To build the A_4 invariant Dirac mass term, we have considered both the lepton doublet Ψ_L and right handed neutrino N_R to transform as triplets, while the Higgs bidoublet transforms as a singlet under the A_4 group. We have considered both the symmetric and asymmetric parts of the Dirac mass term, which is represented by the first and second term of equation (4.4) respectively

$$\mathcal{L}_D = g_1 N_R \Phi(Y\bar{\Psi}_L)_{3_S} + g_2 N_R \Phi(Y\bar{\Psi}_L)_{3_A} . \quad (4.4)$$

Where g_1 and g_2 are some adjustable parameters of the model, and from equation (4.4), we can construct the Dirac mass matrix of the model, which is given in equation (4.5)

$$M_D = v \begin{pmatrix} 2g_1 Y_1 & (-g_1 + g_2) Y_3 & (-g_1 - g_2) Y_2 \\ (-g_1 - g_2) Y_3 & 2g_1 Y_2 & (-g_1 + g_2) Y_1 \\ (-g_1 + g_2) Y_2 & (-g_1 - g_2) Y_1 & 2g_1 Y_3 \end{pmatrix} . \quad (4.5)$$

Where $v = 246$ GeV is the V.E.V of the bidoublet Φ , and we have considered (g_1, g_2) as a real parameter and their values lie within the range of 10^{-4} to 10^{-2} .

C. Majorana mass term for neutrino

We have assigned a singlet to the scalar triplet Δ_L , and by considering the symmetric nature of the Majorana mass term we can write the Majorana mass term, in the following way:

$$\mathcal{L}_M = N_R^C \Delta_R (Y N_R)_{3_S} . \quad (4.6)$$

From equation (4.6), we have constructed the Majorana mass matrix. In equation (4.7), v_R is the V.E.V of the scalar triplet Δ_R , and its value lies in the range of 1 TeV to 100 TeV.

$$M = v_R \begin{pmatrix} 2Y_1 & -Y_3 & -Y_2 \\ -Y_3 & 2Y_2 & -Y_1 \\ -Y_2 & -Y_1 & 2Y_3 \end{pmatrix} . \quad (4.7)$$

D. N-S mixing term

The sterile fermion S_i ($i = 1, 2, 3$) and the scalar doublet χ_R both transform as singlets under the A_4 group, and the scalar doublet χ_R is responsible for $N - S$ mixing. For simplicity purposes, we have only considered the symmetric part of the $N - S$ mixing term, which is given in the equation (4.8)

$$M_N = f(\bar{N}_R Y)_{3_S} \chi_R S . \quad (4.8)$$

Where f is a complex, adjustable parameter of the model, it's real and imaginary values lie within the range of 10^{-5} to 10^{-3} . From the above equation, we have constructed the $N - S$ mixing mass matrix. Which is given in equation (4.9)

$$M_N = v' f \begin{pmatrix} 2Y_1 & -Y_3 & -Y_2 \\ -Y_3 & 2Y_2 & -Y_1 \\ -Y_2 & -Y_1 & 2Y_3 \end{pmatrix} \quad (4.9)$$

where v' is the V.E.V of the scalar doublet χ_R , and we have considered that its value lies within the range of 1 TeV to 100 TeV.

E. Sterile-Sterile ($S - S$) mixing term

This is the Majorana mass term for the sterile fermion, equations (4.10) and (4.11), represent the $S - S$ mixing mass term and the mass matrix respectively. We have taken μ_S within the range of 10 keV to 50 keV.

$$M_S = \mu_S (S^T S) . \quad (4.10)$$

$$M_S = \mu_S \begin{pmatrix} 1 & 0 & 0 \\ 0 & 0 & 1 \\ 0 & 1 & 0 \end{pmatrix} . \quad (4.11)$$

V. EXTENDED INVERSE SEESAW MECHANISM

Spontaneous symmetry breaking of the Yukawa Lagrangian term given in equation (4.1) gives rise to a 9×9 mass matrix, which is given in equation 5.1

$$\begin{pmatrix} 0 & 0 & M_D \\ 0 & \mu_S & M \\ M_D^T & M^T & M_N \end{pmatrix} . \quad (5.1)$$

By considering the mass hierarchy scale as $M > M_N \gg M_D$ we can block diagonalize this 9×9 matrix, and we will finally obtain the mass matrices for the light neutrino, sterile fermion, and right handed neutrino which is given respectively in equations (5.2) .

$$\begin{aligned} m_\nu &= M_D M^{-1} \mu_S (M_D M^{-1})^T \\ m_S &= \mu_S - M M_R^{-1} M^T \\ m_R &= M_R . \end{aligned} \quad (5.2)$$

To obtain the eigenvalues we further diagonalized the matrices given in equation (5.2) by their respective unitary matrices as follows

$$\begin{aligned} \hat{m}_\nu &= U_\nu^\dagger m_\nu U_\nu^* = \text{diag}(m_{\nu_1}, m_{\nu_2}, m_{\nu_3}) \\ \hat{m}_S &= U_S^\dagger m_S U_S^* = \text{diag}(m_{S_1}, m_{S_2}, m_{S_3}) \\ \hat{m}_R &= U_N^\dagger m_R U_N^* = \text{diag}(m_{R_1}, m_{R_2}, m_{R_3}) . \end{aligned} \quad (5.3)$$

The complete mixing matrix responsible for diagonalizing the 9 mass matrix given in the equation 5.1 is shown bellow [49, 50, 52]

$$\mathbf{V} = \begin{pmatrix} V^{\nu\nu} & V^{\nu S} & V^{\nu N} \\ V^{S\nu} & V^{SS} & V^{SN} \\ V^{N\nu} & V^{NS} & V^{NN} \end{pmatrix} = \begin{pmatrix} (1 - \frac{1}{2} X X^\dagger) U_\nu & (X - \frac{1}{2} Z Y^\dagger) U_S & Z U_N \\ -X U_\nu & (1 - \frac{1}{2} (X^\dagger X + Y Y^\dagger)) U_S & (Y - \frac{1}{2} X^\dagger Z) U_N \\ y^* X^\dagger U_\nu & -Y^\dagger U_S & (1 - \frac{1}{2} Y^\dagger Y) U_N \end{pmatrix} \quad (5.4)$$

where $X = M_D M^{-1}$, $Y = M M_N^{-1}$, $Z = M_D M_N^{-1}$, and $y = M^{-1} M_S$

Where $U_\nu = V_l^\dagger V_\nu$, but in this model we have considered the charged lepton mass basis is diagonal i.e. V_l is a identity matrix so usually $V_\nu = U_{PMNS}$. The matrix U_{PMNS} is a unitary matrix and it can be parametrized by using three mixing angle and three phase, among which one is a Dirac CP phase denoted as δ_{CP} and two are Majorana phases (α, β) . By using standard parametrization, we can write the U_{PMNS} matrix in the following way

$$U_{PMNS} = \begin{pmatrix} c_{12}c_{13} & s_{12}c_{13} & s_{13}e^{-i\delta_{CP}} \\ -s_{12}c_{23} - c_{12}s_{23}s_{13}e^{i\delta_{CP}} & c_{12}c_{23} - s_{12}s_{23}s_{13}e^{i\delta_{CP}} & s_{23}c_{13} \\ s_{12}s_{23} - c_{12}c_{23}s_{13}e^{i\delta_{CP}} & -c_{12}s_{23} - s_{12}c_{23}s_{13}e^{i\delta_{CP}} & c_{23}c_{13} \end{pmatrix} \cdot \begin{pmatrix} 1 & 0 & 0 \\ 0 & e^{i\alpha} & 0 \\ 0 & 0 & e^{i\beta} \end{pmatrix}. \quad (5.5)$$

Where c_{ij} and s_{ij} stands for $\cos \theta_{ij}$ and $\sin \theta_{ij}$, respectively. One can represents all the mixing angles in terms of the elements of the U_{PMNS} matrix as given in equation (5.6), and their 3σ values are given in the Table IV. We have used those 3σ range for our numerical analysis part.

$$\sin^2 \theta_{13} = |(U_{PMNS})_{13}|^2, \quad \sin^2 \theta_{23} = \frac{|(U_{PMNS})_{23}|}{1 - |(U_{PMNS})_{13}|^2}, \quad \sin^2 \theta_{12} = \frac{|(U_{PMNS})_{12}|^2}{1 - |(U_{PMNS})_{13}|^2} \quad (5.6)$$

The Dirac CP phase, Jarlskog invariant and Majorana phases can also be estimated from U_{PMNS} matrix, and their relations are given in the equation (5.7) and (5.8) respectively

$$J_{CP} = \text{Im}[U_{e1}U_{\mu 2}U_{e2}^*U_{\mu 1}^*] = s_{23}c_{23}s_{12}c_{12}s_{13}c_{13}^2 \sin \delta_{CP} \quad (5.7)$$

$$\text{Im}[U_{e1}^*U_{e2}] = c_{12}s_{12}c_{13}^2 \sin \alpha, \quad \text{Im}[U_{e1}^*U_{e3}] = c_{12}s_{13}c_{13} \sin(\beta - \delta_{CP}). \quad (5.8)$$

oscillation parameter	for normal hierarchy	for inverted hierarchy
$\sin^2 \theta_{12}$	0.270 \rightarrow 0.341	0.270 \rightarrow 0.341
$\sin^2 \theta_{23}$	0.408 \rightarrow 0.603	0.412 \rightarrow 0.613
$\sin^2 \theta_{13}$	0.02052 \rightarrow 0.02398	0.02048 \rightarrow 0.02416
δ_{CP}	144 \rightarrow 350	194 \rightarrow 344
$\frac{\Delta m_{21}^2}{10^{-5}}$	6.82 \rightarrow 8.03	6.82 \rightarrow 8.03
$\frac{\Delta m_{3l}^2}{10^{-3}}$	+2.427 \rightarrow 2.590	-2.570 \rightarrow -2.406

TABLE IV: 3σ values of oscillation parameter

VI. NON-UNITARY EFFECT

The PMNS matrix is responsible for diagonalizing the light neutrino mass matrix, but in the case of the extended inverse seesaw mechanism, due to the mixing between light and heavy neutrinos even after the diagonalization of the light neutrino mass matrix, we get off-diagonal terms. The complete 9×9 diagonalizing matrix given in the equation (5.4) can be decomposed in the following way [53, 54]

$$\mathbf{V} = \begin{pmatrix} \mathbf{V}_{3 \times 3} & \mathbf{V}_{6 \times 3} \\ \mathbf{V}_{6 \times 3} & \mathbf{V}_{6 \times 6} \end{pmatrix}. \quad (6.1)$$

The PMNS matrix $\mathbf{V}_{3 \times 3} = (1 - \eta)U_\nu$ is responsible for diagonalizing the light neutrino mass matrix and it is not a unitary matrix. The 3×3 hermitian matrix $\eta = \frac{1}{2}XX^\dagger$ is known as the deviation from non-unitarity, which only depends on the Dirac and Majorana matrices of the model. From different experiments upper bounds [55] on the elements of this hermitian matrix have been found and it is given below

$$\eta \leq \begin{pmatrix} 2.5 \times 10^{-3} & 2.4 \times 10^{-5} & 2.7 \times 10^{-3} \\ 2.4 \times 10^{-5} & 4.0 \times 10^{-4} & 1.2 \times 10^{-3} \\ 2.7 \times 10^{-3} & 1.2 \times 10^{-3} & 5.6 \times 10^{-3} \end{pmatrix} \quad (6.2)$$

Due to this non-unitary matrix, the Jarlskog invariant term gets modified, and it can be written in the following way

$$J_{\alpha\beta}^{ij} = \text{Im}(\mathbf{V}_{\alpha i} \mathbf{V}_{\beta j} \mathbf{V}_{\alpha i}^* \mathbf{V}_{\beta j}^*) \approx J_{CP} + \Delta J_{\alpha\beta}^{ij} \quad (6.3)$$

where $\alpha \neq \beta$ and they represent the charged leptons (e, μ, τ), $i \neq j$ and can take the value 1, 2, 3. The first term in the equation (6.3), represents the effect on CP-violation due to the unitary PMNS matrix and the second term represents the contribution to CP- violation due to non-unitary term.

$$\Delta_{\alpha\beta}^{ij} \approx - \sum_{\gamma=e,\mu,\tau} \text{Im}(\eta_{\alpha\gamma} U_{\alpha i} U_{\beta j} U_{\alpha j}^* U_{\beta i}^* + \eta_{\beta\gamma} U_{\alpha i} U_{\gamma j} U_{\alpha j}^* U_{\beta i}^* + \eta_{\alpha\gamma}^* U_{\alpha i} U_{\beta j} U_{\gamma j}^* U_{\beta i}^* + \eta_{\beta\gamma}^* U_{\alpha i} U_{\beta j} U_{\alpha j}^* U_{\gamma i}^*) .$$

Usually, J_{CP} becomes equal to zero when δ_{CP} and $\sin\theta_{13}$ tend to zero but when we consider non-unitary effects Jarlskog invariant term remains non-zero even if δ_{CP} and $\sin\delta_{CP}$ become zero.

VII. NEUTRINOLESS DOUBLE BETA DECAY

Neutrinoless double beta ($0\nu\beta\beta$) is a very fascinating phenomena in which a nucleus undergoes two successive beta decays without emitting any neutrino in the final process. This hypothetical nuclear decay process has not been observed yet. It is a type of beta decay in which two neutrons in the nucleus

simultaneously convert into two protons, emitting two electrons but no accompanying neutrinos. The process can be denoted in the following way

$$N(A, Z) \rightarrow N(A, Z + 2) + 2e^-$$

The process violates conservation of the lepton number, which is an accidental symmetry of the standard model. Observation of such decay would imply that neutrinos are their own antiparticles and have a Majorana nature, meaning that the neutrino and antineutrino are indistinguishable. There are several processes which contribute to the $0\nu\beta\beta$ decay in this model. These processes are discussed below

1. *Contribution due to $W_L - W_L$ current*

In case of $W_L - W_L$ mediation, there are three possible contributions and among them popular contribution to $0\nu\beta\beta$ decay is the standard contribution i.e. contribution due to the exchange of light Majorana neutrino and the other two contributions are due to the exchange of right handed and sterile neutrino, which is also known as the non-standard contribution.

2. *Contribution due to $W_R - W_R$ current*

In case when the mediator is purely right-handed current ($W_R - W_R$), there are three potential contributions to neutrinoless double beta decay ($0\nu\beta\beta$). These contributions arise from the exchange of light neutrinos, right-handed, and sterile neutrinos.

3. *Contribution due to $W_L - W_R$ current*

In case of $W_L - W_R$ mediation, we can have two type of mixed helicity Feynman diagram, which is known as the λ and η diagram.

4. *Contribution due to charged Higgs boson*

The left and right handed doubly charged Higgs boson namely $\Delta_{L,R}$ also contribute to the $0\nu\beta\beta$ decay but its contribution is negligible as compared to other processes.

The Feynman diagram and amplitude of all the above mentioned processes are given in the Appendix A.

VIII. NUMERICAL ANALYSIS AND RESULTS

In case of Extended inverse seesaw mechanism the light neutrino mass matrix is given by

$$m_\nu = M_D M^{-1} \mu_S (M_D M^{-1})^T \quad (8.1)$$

We can also write light neutrino mass matrix in terms of U_{PMNS} matrix in the following way

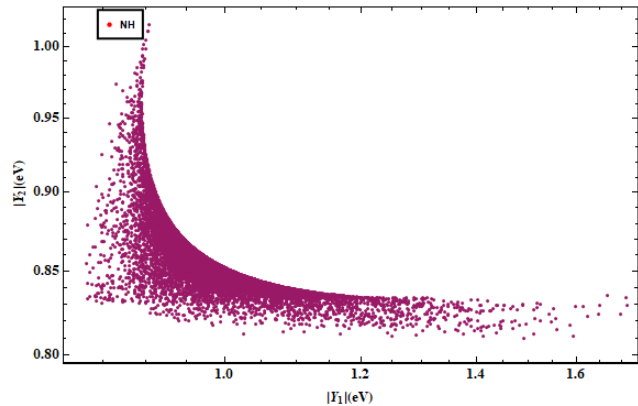
$$m_\nu = U_{PMNS} m_{dig} U_{PMNS}^\dagger \quad (8.2)$$

After constructing the mass matrices utilizing the multiplication rules of the A_4 group, we incorporated these matrices into equation (8.1) to derive the light neutrino mass matrix in terms of Yukawa couplings. To further analyze this, we computed the values of Yukawa couplings using the 3σ values of oscillation parameters, which were inserted into equation (8.2). Subsequently, we equated equations (8.1) and (8.2) to determine the unknown values of the Yukawa coupling. As seen in Figure 1a, the majority of the estimated values for Y_1 and Y_2 lie between 0.7 and 1.4 and between 0.7 and 1, respectively also from Figure 1b we observed that most of the Y_3 values lie from 0.60 to 0.70. Further analysis of Figures 1c and 1d reveals analogous results for (Y_1, Y_2, Y_3) in the case of the IH. Table V provides Yukawa coupling values.

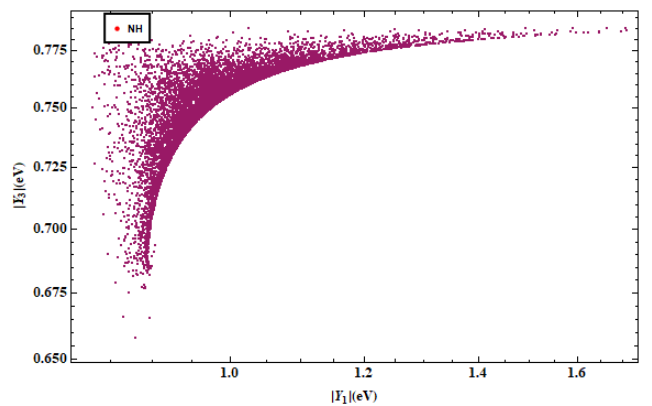
Yukawa coupling	for NH	for IH
Y_1	0.83 – 1.71	0.82 – 1.79
Y_2	0.81 – 1.02	0.80 – 1.01
Y_3	0.66 – 0.78	0.66 – 0.78

TABLE V: Yukawa coupling values for NH and IH

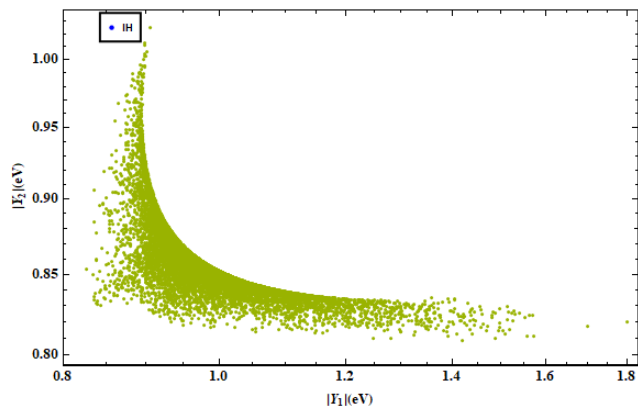
Furthermore with the use of the $\Gamma(3)$ modular group of weight two, our framework can have a total of three modular forms. The three Yukawa couplings in the model are correspond to these modular forms. The motivation behind utilizing the modular group is to minimize the necessity of introducing an additional field, commonly known to as a "flavon", for breaking the discrete flavor symmetry. Within modular symmetry, the modulus τ is responsible for braking the discrete flavor symmetry. We calculated the values of the modulus τ by employing the q expansion of the modular form as given in equation (3.3). We have computed both the absolute value of the modulus τ and its real and imaginary components from our model. From figures 2a and 2c, we observed that absolute value of τ range from 1 – 1.4 for both NH and IH. Additionally, Figures 2b and 2d indicate that the preferred range for the real part of τ falls within $[-1, -0.5]$ and $[-.1, 0.6]$ for the NH scenario, and within $[-1, -0.6]$ and $[0.1, 0.8]$ for the IH scenario.



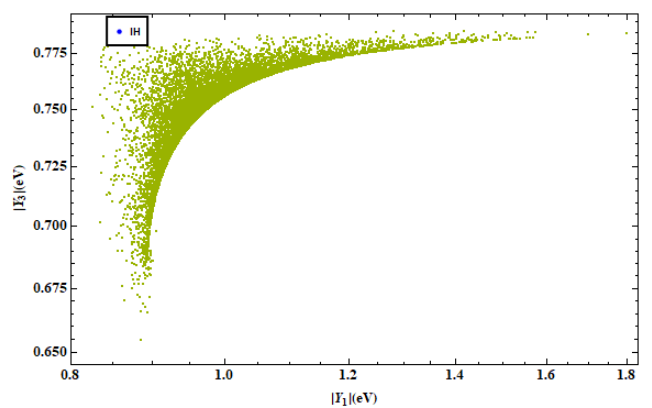
(a) $|Y_1|$ vs $|Y_2|$



(b) $|Y_1|$ vs $|Y_3|$



(c) $|Y_1|$ vs $|Y_2|$

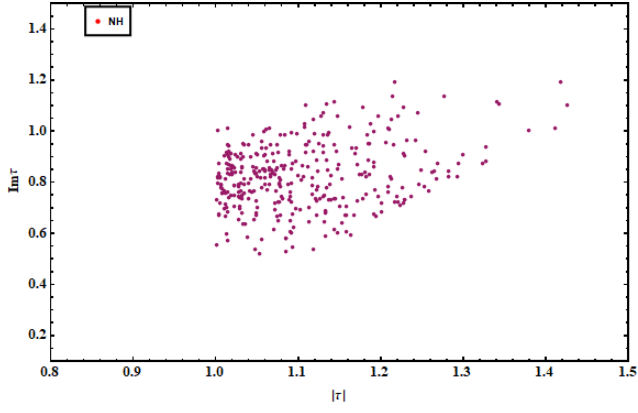


(d) $|Y_1|$ vs $|Y_3|$

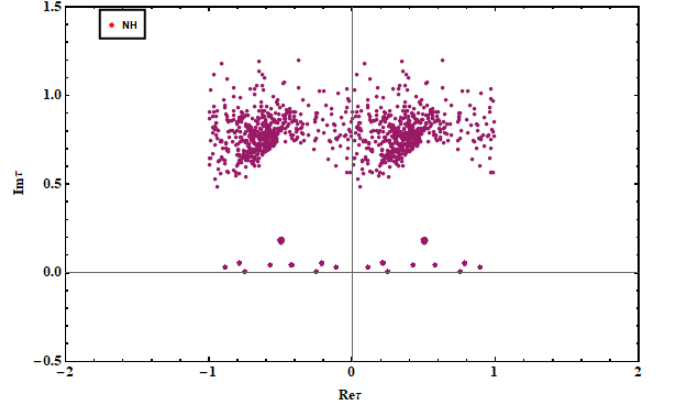
FIG. 1: Top two Figure shows parameter space of Yukawa coupling for NH and the bottom two figure shows parameter space of Yukawa coupling for IH

A. Active neutrino masses

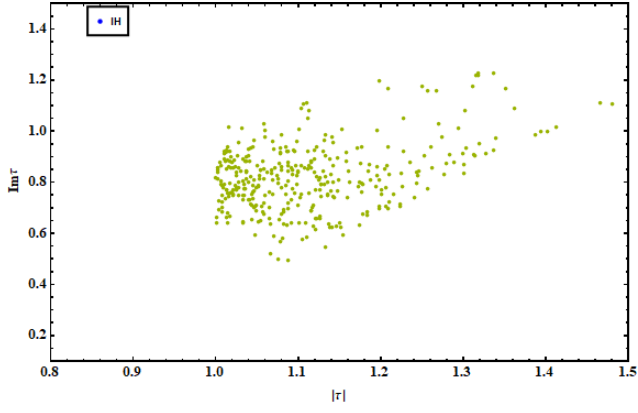
We have plotted a graph depicting the relationship between the sum of neutrino masses and the lightest neutrino mass, considering both the normal and inverted hierarchy. It appears that majority of the calculated values lie below the experimental bound. This experimental bound is represented by a horizontal line on the graph. To verify the consistency of the model we have also plotted mixing angle calculated from the model against the lightest neutrino mass for both NH and IH. Figure 4b shows the variation of $\sin^2 \theta_{23}$ and $\sin^2 \theta_{12}$ respectively with the lightest neutrino mass and have observed that most of the data fall within the experimental 3σ range. In figure 4a, we observed that less number of data points fall within the 3σ range of $\sin^2 \theta_{13}$, as compared to the other mixing angle which indicated that the present model is less predictive towards the reactor angle. We have observed similar kind of results for IH also, which is shown in the figure 4d and 4c. We have also calculated the value of the two Majorana phases and δ_{CP} from our model. From Figure 3c, it is observed that the Majorana phase α lie within the range of $[0^0 - 50^0]$ and $[300^0 - 350^0]$, also δ_{CP} values is same as the Majorana phase α .



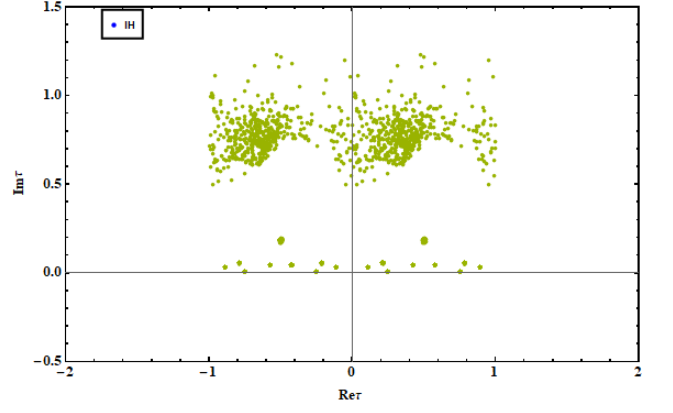
(a) Variation of $|\tau|$ and $\text{Im}\tau$



(b) Variation of $\text{Re}\tau$ and $\text{Im}\tau$



(c) Variation of $|\tau|$ and $\text{Im}\tau$



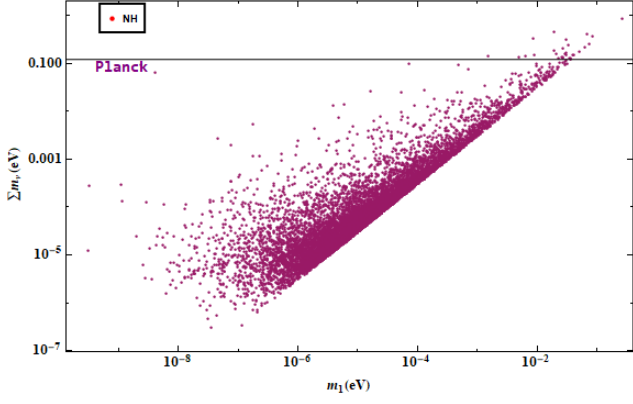
(d) Variation of $\text{Re}\tau$ vs $\text{Im}\tau$

FIG. 2: The top and bottom two Figure shows the parameter space of absolute value of modulus τ and its real and imaginary part for NH and IH respectively

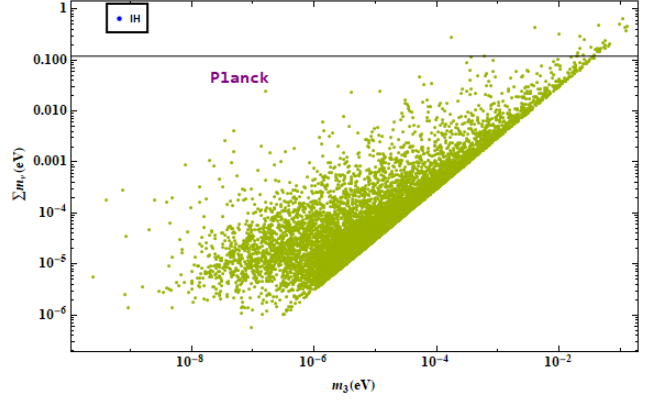
Majorana phase β cover all the values from 0° to 350° and it hold true for both the NH and IH case.

B. Right handed (RH) neutrino mass

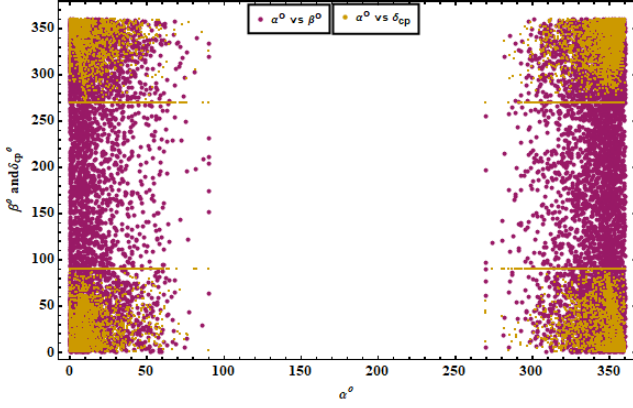
We have assumed that the right handed neutrino is the heavier then the other mass scales, and we have excluded all the right handed neutrino masses bellow 10^{12}eV from consideration. In figure 5a and 5b we can see that all the values fall above 10^{12}eV . To analyzed relation between the RH neutrino masses we have plotted the variation of M_{N_1} against M_{N_2} and M_{N_3} for both NH and IH. In the Figure 5c, we observed that the plot between right handed neutrino mass M_{N_1} and M_{N_2} shows some linear relation among them. However, the data points for the plot between M_{N_1} and M_{N_3} is scattering that is deviating from this linear pattern. By analyzing these two graph, we can concluded that the right handed neutrino mass M_{N_1} is approximately equal to M_{N_2} , while M_{N_3} is the lightest among them, satisfying the condition $M_{N_1} \approx M_{N_2} > M_{N_3}$. This conclusion holds true for both the normal and inverted hierarchy.



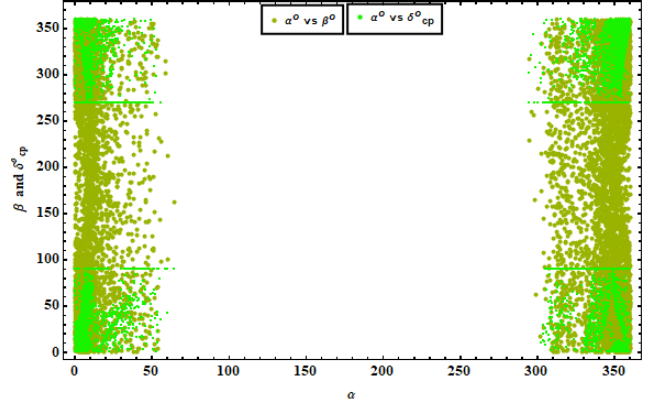
(a) Variation of $\sum m_\nu$ with m_1



(b) Variation of $\sum m_\nu$ with m_3



(c) Parameter space of δ_{CP} and Majorana phase for NH

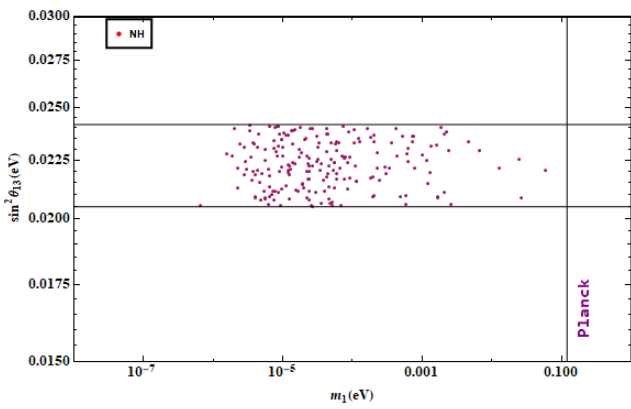


(d) Parameter space of δ_{CP} and Majorana phase for IH

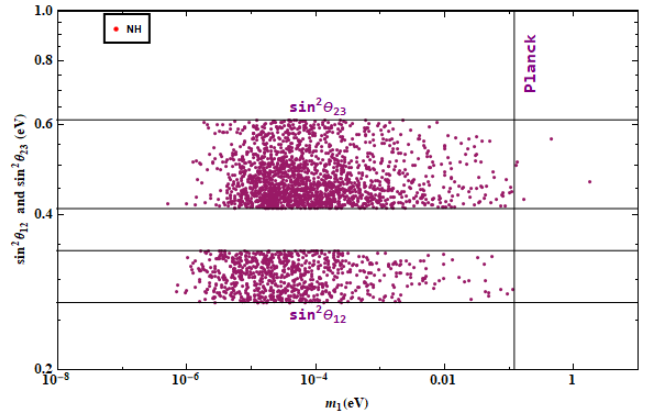
FIG. 3: The top two Figure shows variation of sum of the neutrino masses with the lightest neutrino mass for NH and IH and the bottom two figure shows the parameter space of δ_{CP} and Majorana phases (α and β) for NH and IH

C. Sterile fermion mass

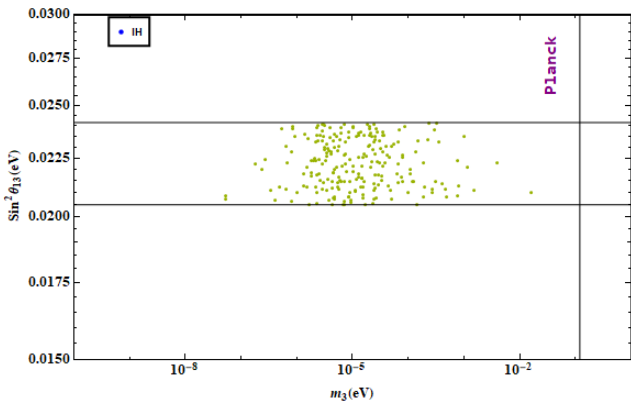
We have plotted a graph between the heaviest sterile fermion mass and the three Yukawa couplings for NH and IH, shown in Figure 6a and 6b. In this plots, the upper horizontal lines indicated that we have excluded all the sterile fermion masses above 10^{12} eV from further consideration. Through a similar analysis, we have studied the correlation between masses of sterile fermions. In the Figure 6c, we have observed scattered data points for the plots M_{S_1} and M_{S_3} , whereas for the plot M_{S_1} against M_{S_2} , data points shows a linear relation. Based on our analysis, we predict that the sterile fermion mass M_{S_1} is greater than or equal to M_{S_2} , and M_{S_3} is the lightest among them, satisfying the condition $M_{S_1} \geq M_{S_2} > M_{S_3}$.



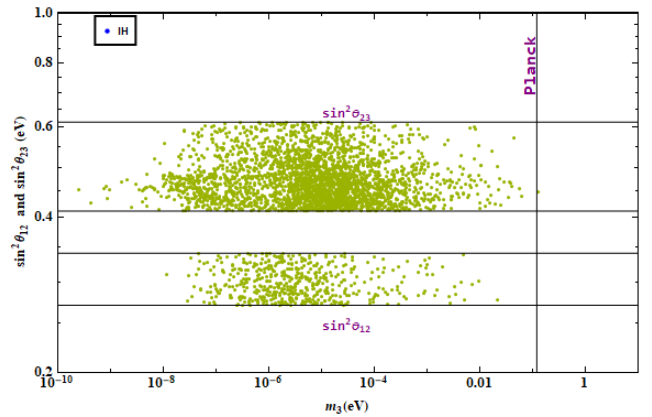
(a) $\sin^2 \theta_{13}$ vs m_1



(b) $\sin^2 \theta_{23}$ and $\sin^2 \theta_{12}$ vs $sum m_1$



(c) $\sin^2 \theta_{13}$ vs m_3



(d) $\sin^2 \theta_{23}$ and $\sin^2 \theta_{12}$ vs m_3

FIG. 4: Figure shows the variation of mixing angles with the lightest neutrino mass for NH and IH

D. Effective neutrino mass and Half life of $0\nu\beta\beta$ decay

In Section VII, we have briefly discussed all the contributions to $0\nu\beta\beta$ decay associated with our model and in this section we have discussed effective mass and its corresponding half-life and done a detailed numerical analysis of all the contributions. We have plotted graphs showing the variation of the effective mass of $0\nu\beta\beta$ decay and its corresponding half-life of $(0\nu\beta\beta)$ decay with the lightest neutrino mass, considering both standard and non-standard contributions. In all the plots, which represent the variation of effective mass with the lightest neutrino mass, the presence of a horizontal line indicates the Planck constraint on the total sum of neutrino masses, while the two vertical lines represent the uncertainty on the effective mass due to nuclear mass matrix and effective mass should be less than this bound. Similarly, in all the figures, related to the half life of $0\nu\beta\beta$ the horizontal line represents the Planck constraint, whereas the two vertical lines indicate the experimental bounds on the half-life for the isotope Xe^{136} . Different experimental bounds on the half-life of $0\nu\beta\beta$ for the isotopes Ge and Xe are given in Table VI. As already mentioned within the left-right asymmetric framework, gauge coupling, g_l and g_r are not equal and their values depend upon the symmetry breaking chain. Due to an unequal

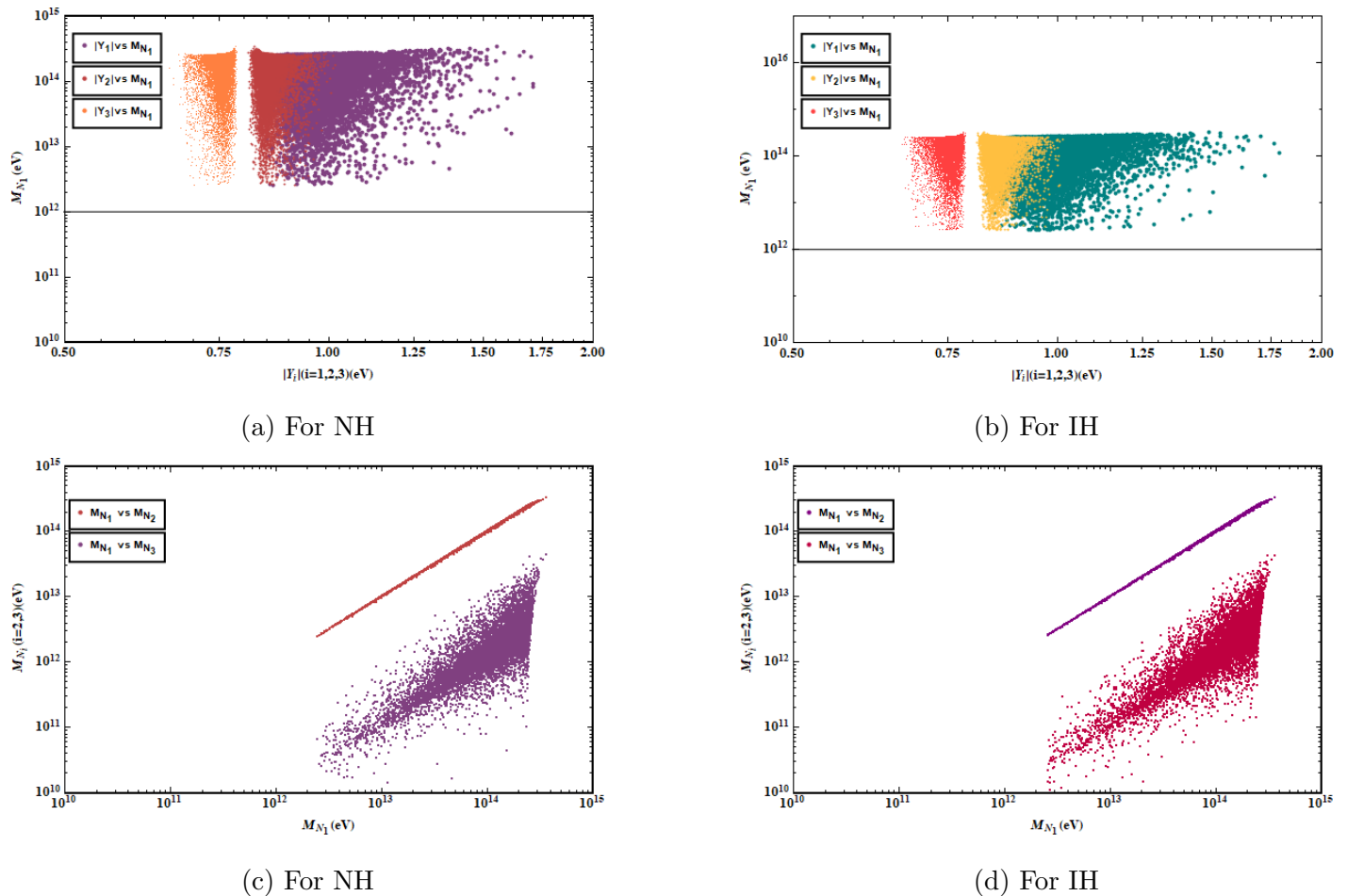
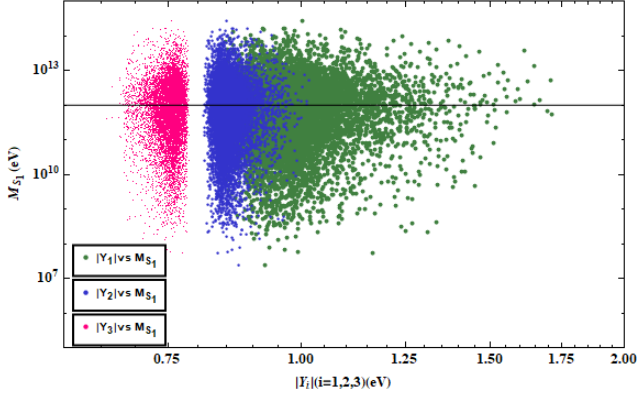


FIG. 5: Top two figure shows variation of Yukawa couplings with the heaviest right handed neutrino mass and the bottom two figure shows the correlation among RH neutrino masses

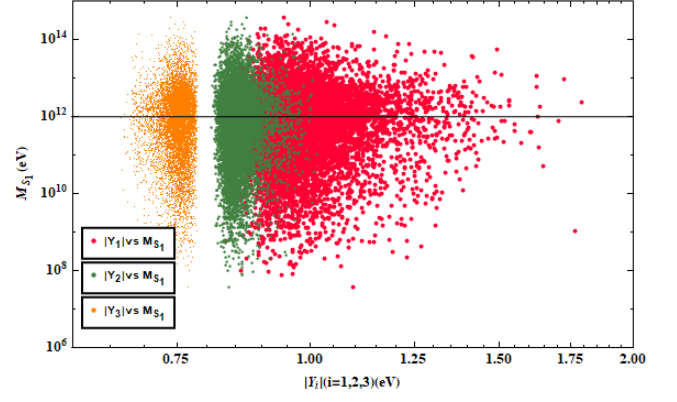
gauge coupling we can see that an extra term ($\frac{g_r}{g_l}$) appears in the calculation of effective Majorana mass and half-life of $0\nu\beta\beta$ decay. We have considered the ratio $\frac{g_r}{g_l}$ equal to 0.6 [56] and the right-handed gauge boson mass W_R of 3 TeV. A detail discussion about the effective Majorana mass and half life of $0\nu\beta\beta$ is given in the Appendix A and B respectively.

Isotope	$76Ge$	$136Xe$	$136Xe$	$136Xe$
$T_{1/2}^{0\nu}[years]$	$> 1.8 \times 10^{26}$	3.5×10^{25}	$> 1.9 \times 10^{25}$	$> 2.3 \times 10^{26}$
Experiment	GERDA [57]	EXO [58]	KamLAND-Zen [59]	EXO + KamLAND-Zen [60]

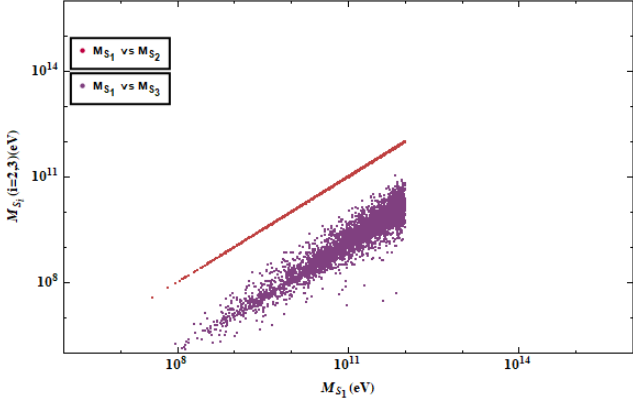
TABLE VI: Experimental bounds on half-life



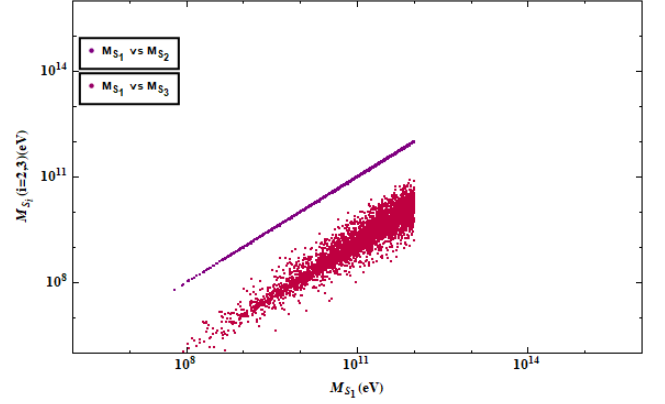
(a) For NH



(b) For IH



(c) For NH



(d) For IH

FIG. 6: Top two Figure shows the variation of Yukawa couplings with the heaviest sterile fermion mass and the bottom two figure shows the correlation among sterile fermion masses

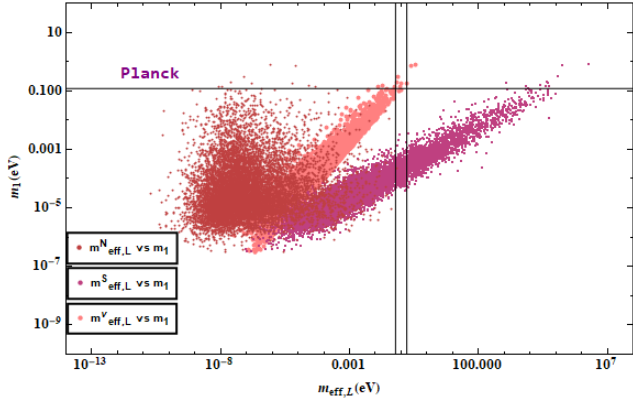
1. Effective mass and half-life due to $W_L - W_L$ current

The effective Majorana mass and life life due to exchange of light neutrino and heavy neutrino in case of $W_L - W_L$ current are given in the equation (8.3) and (8.4) respectively

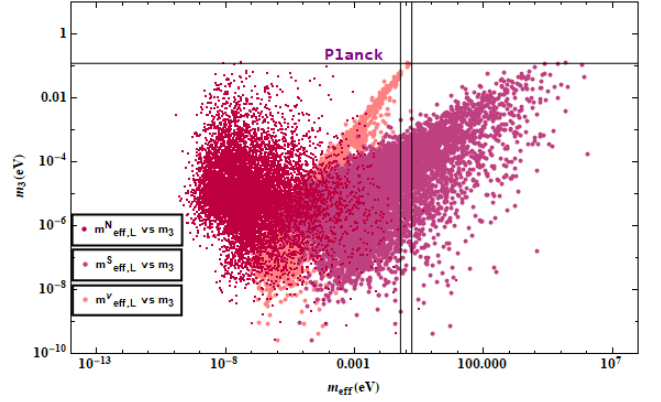
$$m_{ee,L}^\nu = \sum_{i=1}^3 V_{ei}^{\nu\nu^2} m_{\nu i}, \quad m_{ee,L}^N = \sum_{i=1}^3 V_{ei}^{\nu N^2} \frac{|p|^2}{M_{N_i}}, \quad m_{ee,L}^S = \sum_{i=1}^3 V_{ei}^{\nu S^2} \frac{|p|^2}{M_{S_i}}. \quad (8.3)$$

$$[T_{1/2}^{0\nu}]^{-1} = \mathcal{K}_{0\nu} \left[|m_{ee,L}^\nu|^2 + |m_{ee,L}^S + m_{ee,L}^N|^2 \right] \quad (8.4)$$

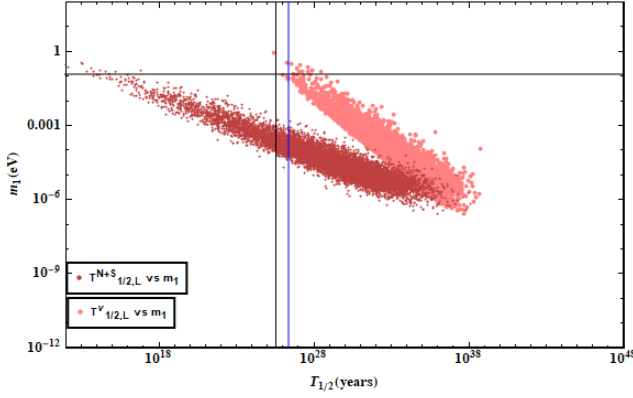
We have calculated the effective Majorana mass and its corresponding half life of $0\nu\beta\beta$ for $W_L - W_L$ mediation due to the exchange of light neutrino, RH neutrino, and sterile neutrino and figure and plotted those calculated values against lightest neutrino mass. In Figure 7a, and 7b we have observed that all the calculated value of effective mass due to light and sterile neutrino fall well below the experimental bound. We have also calculated the half-life of $0\nu\beta\beta$ decay due to light neutrino exchange and due to the exchange of heavy neutrinos for NH and IH, which is shown in the Figure 7c and 7d respectively.



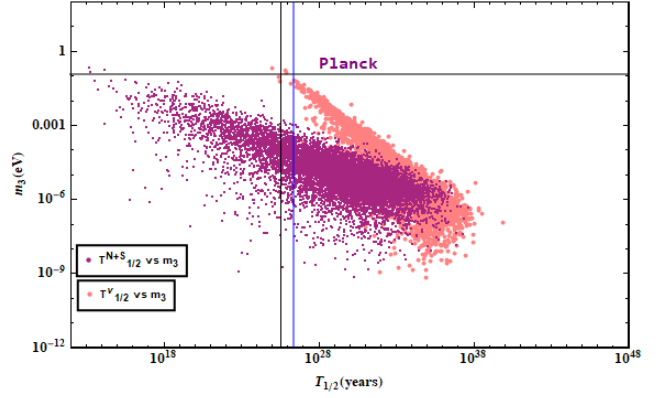
(a) For NH



(b) For IH



(c) For NH



(d) For IH

FIG. 7: Top two figure shows the variation of effective mass with the lightest neutrino mass and the bottom two figure shows the variation of Haff-life of $0\nu\beta\beta$ decay with lightest neutrino mass

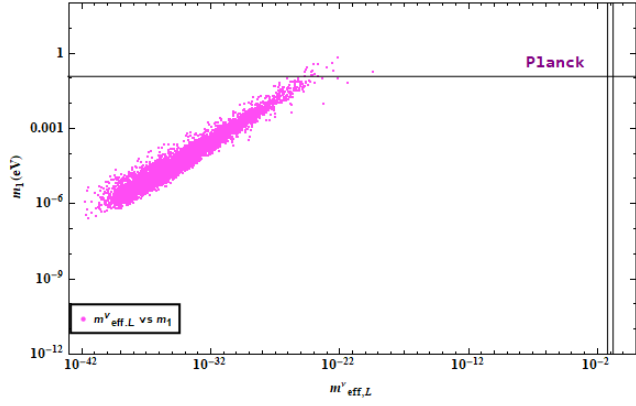
2. Effective mass and half-life due to $W_R - W_R$ current

The effective Majorana mass and life life due to exchange of light neutrino and heavy neutrino in case of purely right handed current are given in the equation (8.5) and (8.6) respectively

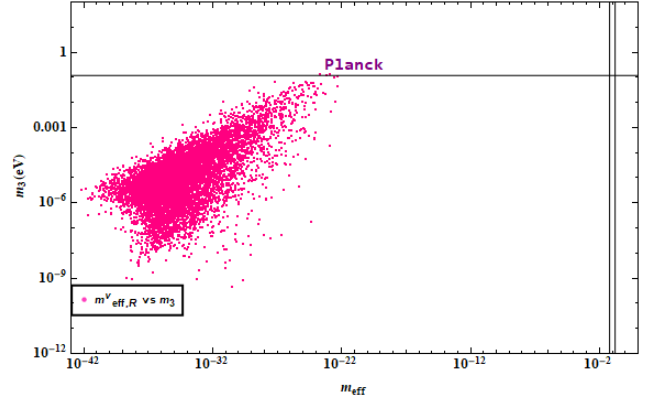
$$\begin{aligned}
 m_{ee,R}^\nu &= \left(\frac{M_{W_L}}{M_{W_R}} \right)^4 \left(\frac{g_r}{g_l} \right)^4 \sum_{i=1}^3 V_{ei}^{N\nu^2} m_{\nu i} \\
 m_{ee,R}^N &= \left(\frac{M_{W_L}}{M_{W_R}} \right)^4 \left(\frac{g_r}{g_l} \right)^4 \sum_{i=1}^3 V_{ei}^{NN^2} \frac{|p|^2}{M_{N_i}} \\
 m_{ee,R}^S &= \left(\frac{M_{W_L}}{M_{W_R}} \right)^4 \left(\frac{g_r}{g_l} \right)^4 \sum_{i=1}^3 V_{ei}^{NS^2} \frac{|p|^2}{M_{S_i}}
 \end{aligned} \tag{8.5}$$

$$[T_{1/2}^{0\nu}]^{-1} = \mathcal{K}_{0\nu} \left[|m_{ee,R}^\nu + m_{ee,R}^S + m_{ee,R}^N|^2 \right] \tag{8.6}$$

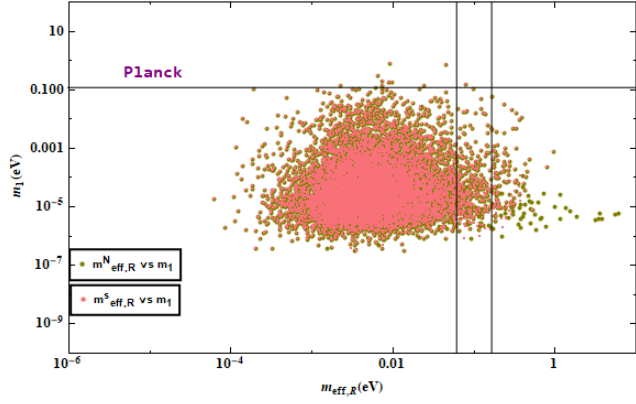
We have calculated the effective Majorana mass and corresponding half-life for the $(0\nu\beta\beta)$ decay mediated by $W_R - W_R$ interactions, considering the exchange of light neutrinos, RH, and sterile neutrinos.



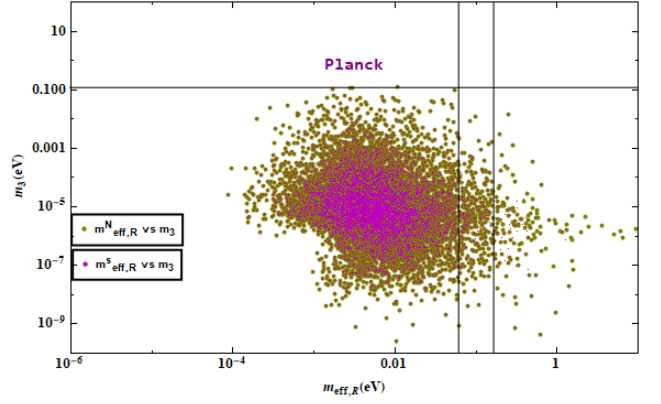
(a) For NH



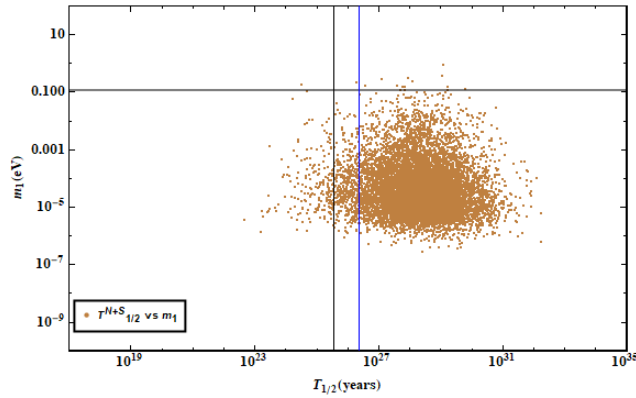
(b) For IH



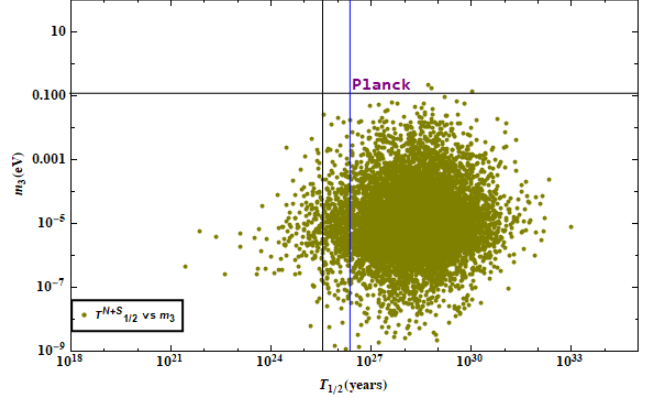
(c) For NH



(d) For IH



(e) For NH



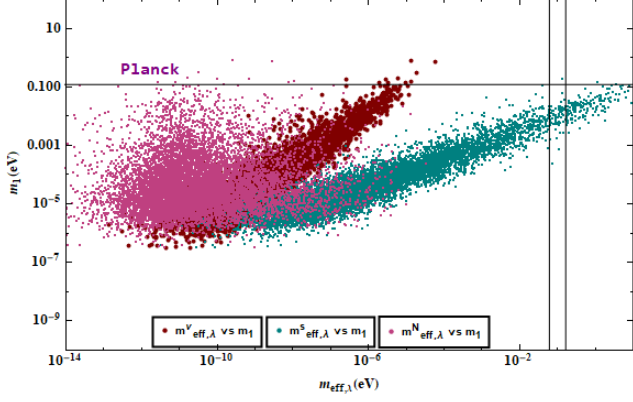
(f) For IH

FIG. 8: Top four figure shows the variation of effective mass with the lightest neutrino mass and the bottom two figure shows the variation of half-life with the lightest neutrino mass

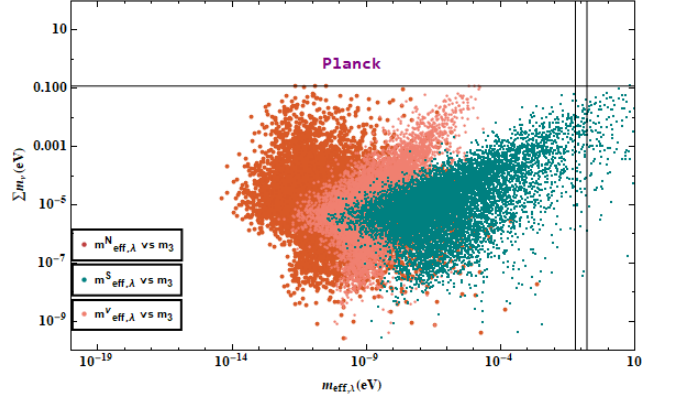
In Figures 8c and 8d, we observed that the calculated effective masses due to RH and sterile neutrino exchanges consistently fall below the experimental bounds. Notably, the contribution from the exchange of light neutrinos via $W_R - W_R$ currents was found to be significantly smaller compared to other mechanisms, resulting in a very large corresponding half-life. Given this negligible contribution, we have omitted it from our total half-life calculations related to $W_R - W_R$ interactions. In Figure 8e and 8f,

we have depicted the calculated half-lives for $(0\nu\beta\beta)$ decay resulting from heavy neutrino exchanges, plotted against the lightest neutrino mass for both NH and IH scenarios.

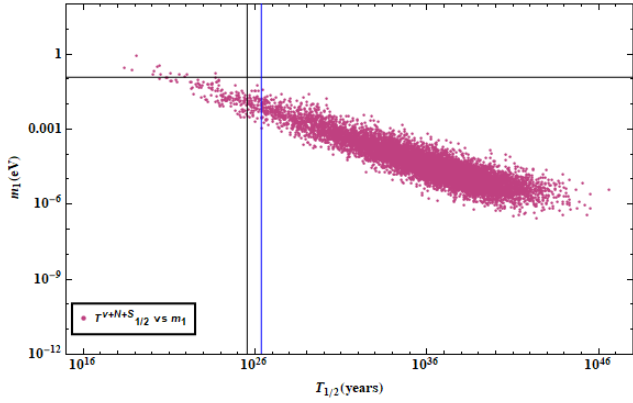
3. Effective mass and half-life due to $W_R - W_L$ current



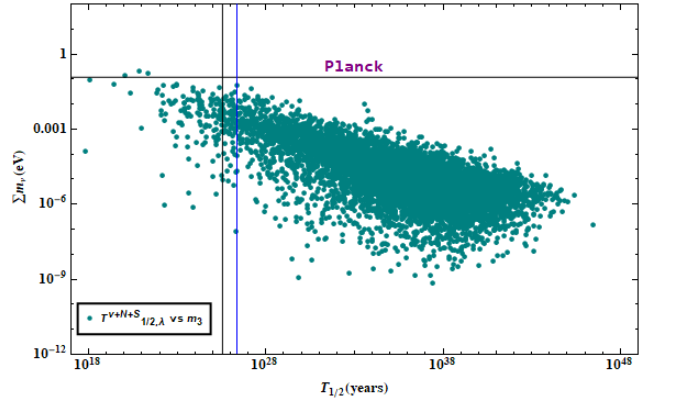
(a) For NH



(b) For IH



(c) For NH



(d) For IH

FIG. 9: Top four figure shows the variation of effective mass with the lightest neutrino mass and the bottom two figure shows the variation of half-life with the lightest neutrino mass

In the present work we have only studied the contribution to $0\nu\beta\beta$ decay due to λ mechanism. The effective Majorana mass and half life due to λ contribution are given in equation (8.7) and (8.8) respectively.

$$\begin{aligned}
 m_{ee,\lambda}^{\nu} &= 10^{-2} \left(\frac{M_{W_L}}{M_{W_R}} \right)^2 \left(\frac{g_r}{g_l} \right)^2 \sum_{i=1,2,3} V_{ei}^{\nu\nu} V_{ei}^{N\nu} |P| \\
 m_{ee,\lambda}^N &= 10^{-2} \left(\frac{M_{W_L}}{M_{W_R}} \right)^2 \left(\frac{g_r}{g_l} \right)^2 \sum_{j=1,2,3} V_{ei}^{\nu N} V_{ej}^{NN} \frac{|p|^3}{M_{N_j}^2} \\
 m_{ee,\lambda}^S &= 10^{-2} \left(\frac{M_{W_L}}{M_{W_R}} \right)^2 \left(\frac{g_r}{g_l} \right)^2 \sum_{k=1,2,3} V_{ek}^{\nu S} V_{ek}^{Ns} \frac{|p|^3}{M_{S_k}^2}
 \end{aligned} \tag{8.7}$$

$$[T_{1/2}^{0\nu}]^{-1} = \mathcal{K}_{0\nu} \left[|m_{ee,\lambda}^\nu + m_{ee,\lambda}^S + m_{ee,\lambda}^N|^2 \right] \quad (8.8)$$

We have plotted the variation of effective mass with the lightest neutrino mass for NH and IH shown in Figure 9a and 9b respectively. We have observed that light and sterile neutrinos contribute large compared to RH neutrino in the calculation of effective mass. We have also calculated the half-life due to λ mechanism and its variation with the lightest neutrino mass is shown in the Figure 9c, 9d for NH and IH respectively.

E. Calculation of non-unitary matrix and J_{CP}

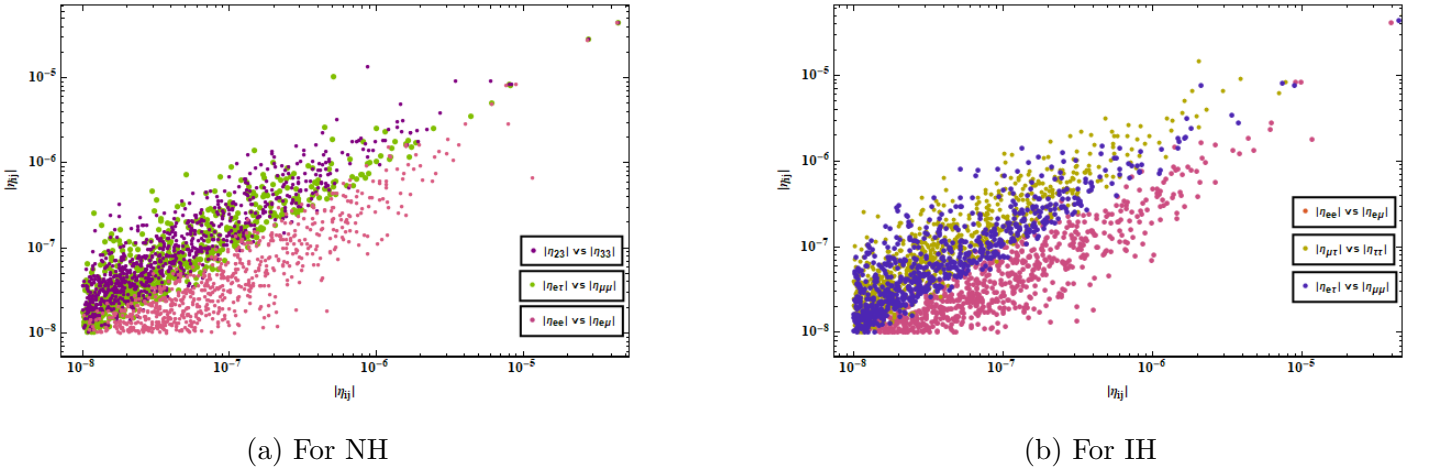


FIG. 10: Parameter space for the elements of the non-unitary matrix

Due to the presence of heavy RH and sterile neutrino we obtain a non-unitary PMNS matrix and the term $\eta = \frac{1}{2}XX^\dagger$ represents the deviation from non-unitarity. Our calculations show that the deviations from unitarity, represented by the elements of this matrix, predominantly fall within the range of 10^{-5} to 10^{-8} , well below the experimental bounds. Table VII shows the calculated upper bounds of elements of the matrix while Figures 10a and 10b illustrate the parameter space for these elements under NH and IH scenarios, respectively. Examining the CP violation term resulting from non-unitarity, we find that $J_{e\mu}^{13}$ is equal to $J_{e\mu}^{32}$ and their values range from -1.7×10^{-6} to 4.4×10^{-6} . We have also get equal value of $J_{e\mu}^{31}$ and $J_{e\mu}^{23}$ and their values varies from -4.4×10^{-6} to 1.7×10^{-6} . Additionally, we observe that the absolute values of $J_{e\tau}^{ij}$ are equal. Similar result is also observed for $J_{\mu\tau}^{ij}$, where $i \neq j$ and it can take values from 1 to 3. Calculated the CP violation term due to non-unitary effect are given in the Table VIII.

η_{ij}	η_{ee}	$\eta_{e\mu}$	$\eta_{e\tau}$	$\eta_{\mu\mu}$	$\eta_{\mu\tau}$	$\eta_{\tau\tau}$
For NH	1.4×10^{-5}	1.5×10^{-5}	1.8×10^{-5}	2.0×10^{-5}	2.1×10^{-5}	2.6×10^{-5}
For IH	3.9×10^{-5}	4.1×10^{-5}	4.4×10^{-5}	4.4×10^{-5}	4.7×10^{-5}	5.1×10^{-5}

TABLE VII: Calculated values of the elements of the non-unitary matrix

$\Delta J_{\alpha\beta}^{ij}$	$\Delta J_{e\mu}^{21}$	$\Delta J_{e\mu}^{13}$	$\Delta J_{e\tau}^{12}$	$\Delta J_{\mu e}^{13}$	$\Delta J_{\mu\tau}^{12}$	$\Delta J_{\tau e}^{31}$
Minimum	-2.69×10^{-6}	-1.7×10^{-6}	-5.5×10^{-6}	-5.8×10^{-6}	-1.1×10^{-6}	-8.4×10^{-7}
Maximum	8.5×10^{-6}	4.4×10^{-6}	1.1×10^{-6}	1.7×10^{-6}	5.0×10^{-7}	2.0×10^{-6}

TABLE VIII: Calculated values of $\Delta J_{\alpha\beta}^{ij}$

IX. CONCLUSION

In this work, we have studied the left-right asymmetric model, where we have used the intermediate gauge group $SU(2)_R \times U(1)_R \times U(1)_{B-L}$ to explore the neutrino masses and mixing by using the $\Gamma(3)$ modular group, which is isomorphic to the A_4 discrete symmetric group. We have developed the model without relying on flavon fields, which is one of the main advantages of modular symmetry. Also, we have described the three Yukawa couplings of our model in terms of modulus τ . For a model to consistence under modular symmetry the absolute value of τ should be greater than 1, and the imaginary part of τ must fall on the upper half of the complex plane. The model satisfies both conditions. We have observed that the majority of the absolute values of τ are greater than 1, while all imaginary components of τ are situated in the upper half of the complex plane, i.e., greater than 0. We have generated the light neutrino mass by using an extended inverse seesaw mechanism and for that purpose, we have introduced one sterile fermion per generation. The model predicts the sum of neutrino masses, with values well below experimental bounds for both NH and IH. Specifically, for NH, the sum ranges from 1.7 to 1.66×10^{-7} , and for IH, it varies from 0.72 to 1.8×10^{-8} . The model is also successful in estimating a satisfactory result for the mixing angles as most of the analytical values fall within the 3σ range. We have also examined the mass hierarchy of heavy RH and sterile neutrinos, observing consistent patterns: $M_{N_1} \approx M_{N_2} > M_{N_3}$ for RH neutrinos and $M_{S_1} \geq M_{S_2} > M_{S_3}$ for sterile fermions, valid for both NH and

IH scenarios. Additionally, we calculated effective mass and half-lives due to the mediation of $W_L - W_L$, $W_R - W_R$, and λ contribution due to the mediation of $W_L - W_R$. We have observed that the analytical formula for effective mass get modified for $W_R - W_R$ and $W_L - W_R$ mediation and depend on the ratio $\frac{g_r}{g_l}$. All the calculated value of effective mass parameter and its corresponding half-lives due to standard and non-standard contribution are found to lie in the experimental allowed region for both the NH and IH case. Furthermore, we analyzed deviations from unitarity in the relevant matrix elements, finding them within the range of 10^{-5} to 10^{-8} . The model have provided a satisfactory result in the calculation of sum of the neutrino masses and neutrino oscillation parameter and have also successful in calculating the effective mass and half-life of $0\nu\beta\beta$ decay.

Appendix A: Feynman diagram and Feynman amplitude for different contribution to $0\nu\beta\beta$ decay

a. Contribution due to $W_L - W_L$ current

The Feynman diagram associated with those contributions are given in Figure 11 and the associated Feynman amplitude and its corresponding lepton number violating (LNV) particle physics parameter are given in the equation (A1), and (A2) respectively.

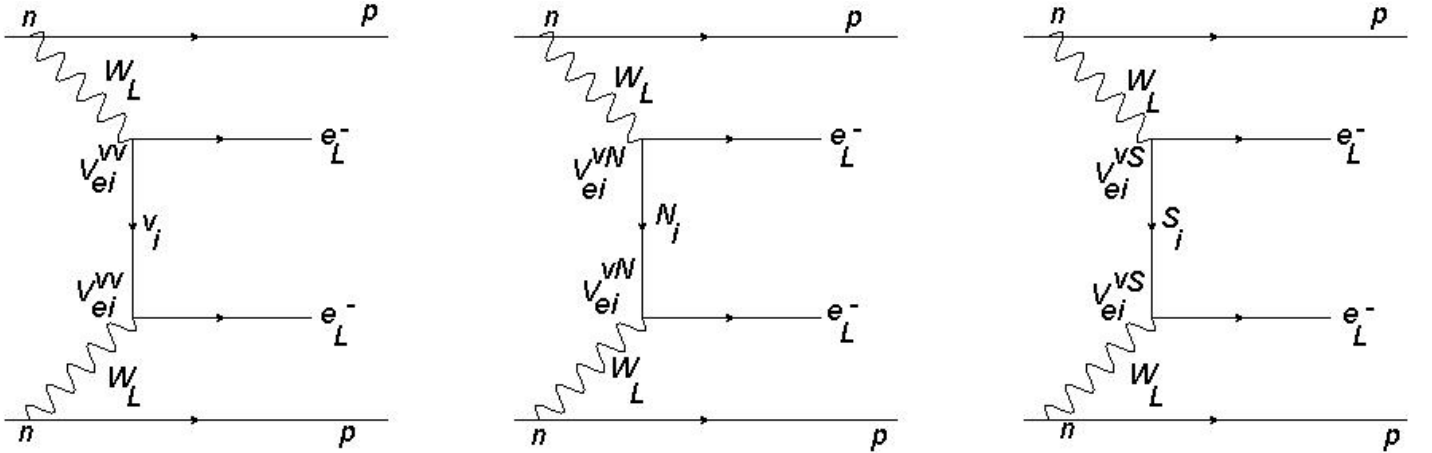


FIG. 11: Feynman diagram for $W_L - W_L$ mediation

$$\mathcal{A}_{LL}^\nu \propto G_R^2 \sum_{i=1,2,3} \frac{V_{ei}^{\nu\nu} m_{\nu_i}}{p^2}, \quad \mathcal{A}_{LL}^N \propto G_F^2 \sum_{i=1,2,3} \left(-\frac{V_{ei}^{\nu N^2}}{M_{N_i}} \right), \quad \mathcal{A}_{LL}^S \propto G_F^2 \sum_{i=1,2,3} \left(-\frac{V_{ek}^{\nu S^2}}{M_{S_k}} \right) \quad (\text{A1})$$

where $G_F = 1.2 \times 10^{-5} \text{GeV}^{-2}$ is the Fermi coupling constant.

$$|\eta_{LL}^\nu| = \sum_{i=1,2,3} \frac{V_{ei}^{\nu\nu^2} m_{\nu_i}}{m_e}, \quad |\eta_{LL}^N| = m_p \sum_{i=1,2,3} \frac{V_{ei}^{\nu N^2}}{M_{N_i}}, \quad |\eta_{LL}^S| = m_p \sum_{i=1,2,3} \frac{V_{ei}^{\nu S^2}}{M_{S_i}} \quad (\text{A2})$$

b. Contribution due to $W_R - W_R$ current

The Feynman diagram for those contributions are given in Figure 12. Equations(A3) and (A4) provide the amplitude of those diagrams and LNV parameters respectively.

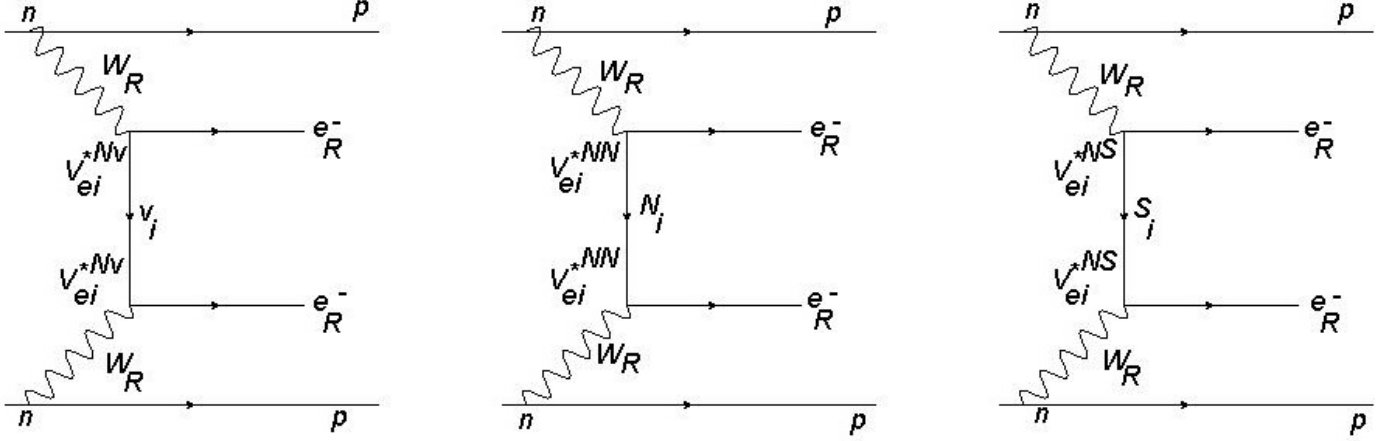


FIG. 12: Feynman diagram for $W_R - W_R$

$$\mathcal{A}_{RR}^\nu \propto G_F^2 \sum_{i=1,2,3} \left(\frac{M_{W_L}}{M_{W_R}}\right)^4 \left(\frac{g_r}{g_l}\right)^4 \frac{V_{ei}^{N\nu^2} m_{\nu_i}}{p^2}$$

$$\mathcal{A}_{RR}^N \propto G_F^2 \sum_{J=1,2,3} \left(\frac{M_{W_L}}{M_{W_R}}\right)^4 \left(\frac{g_r}{g_l}\right)^4 \left(-\frac{V_{ej}^{NN^2}}{M_{N_j}}\right) \quad (\text{A3})$$

$$\mathcal{A}_{RR}^S \propto G_F^2 \sum_{k=1,2,3} \left(\frac{M_{W_L}}{M_{W_R}}\right)^4 \left(\frac{g_r}{g_l}\right)^4 \left(-\frac{V_{ek}^{NS^2}}{M_{S_k}}\right)$$

$$|\eta|_{RR}^\nu = \sum_{i=1,2,3} \left(\frac{M_{W_L}}{M_{W_R}}\right)^4 \left(\frac{g_r}{g_l}\right)^4 \frac{V_{ei}^{N\nu^2} m_{\nu_i}}{m_e}$$

$$|\eta|_{RR}^N = \sum_{i=1,2,3} m_p \left(\frac{M_{W_L}}{M_{W_R}}\right)^4 \left(\frac{g_r}{g_l}\right)^4 \left(\frac{V_{ei}^{NN^2}}{M_{N_i}}\right) \quad (\text{A4})$$

$$|\eta|_{RR}^S = \sum_{i=1,2,3} m_p \left(\frac{M_{W_L}}{M_{W_R}}\right)^4 \left(\frac{g_r}{g_l}\right)^4 \left(\frac{V_{ei}^{NS^2}}{M_{S_i}}\right)$$

c. Contribution due to $W_L - W_R$ current

In case of $W_L - W_R$ mediation, we can have two type of mixed helicity Feynman diagram, which is known as the λ and η diagram. The Feynman diagram associated with those contribution is given in the Figure 13 and 14 respectively.

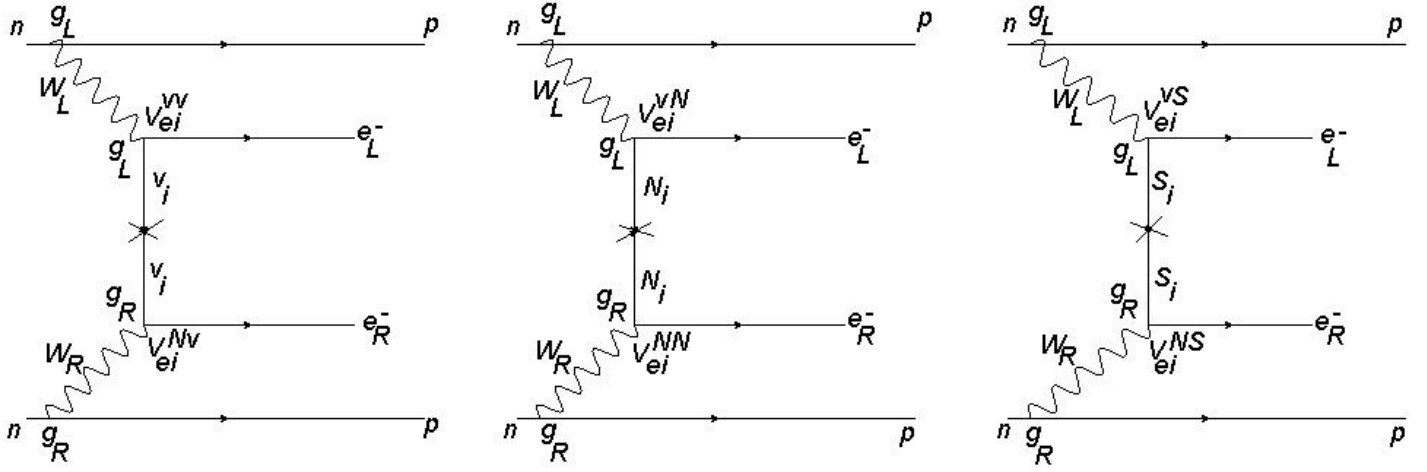


FIG. 13: Feynman diagram for λ

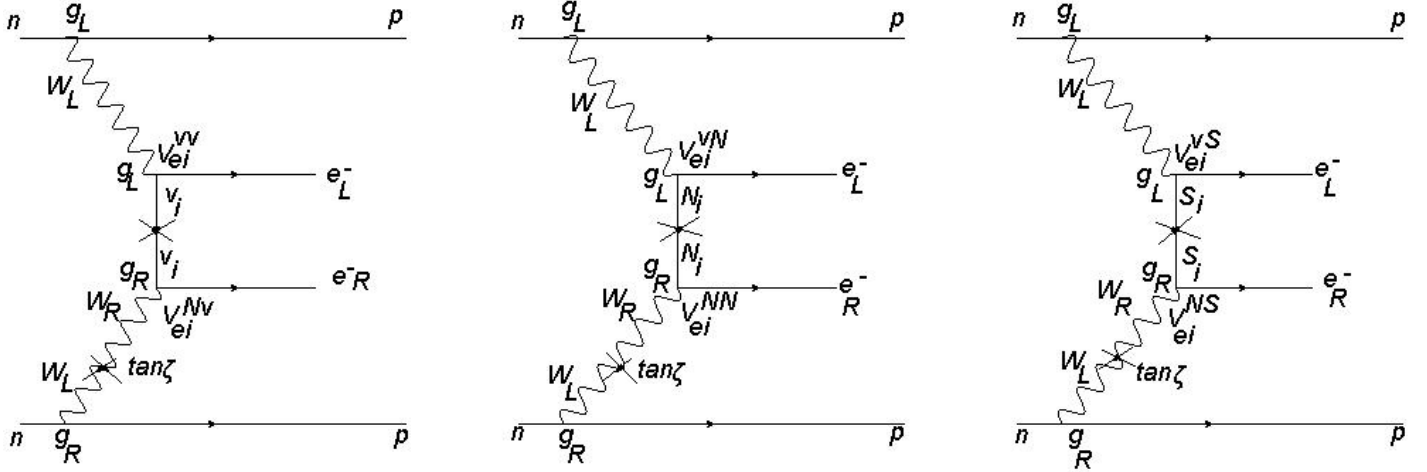


FIG. 14: Feynman diagram for η

1 Feynman amplitudes for λ - mechanism

$$\begin{aligned}
 \mathcal{A}_\lambda^{\nu} &\propto G_F^2 \left(\frac{M_{W_L}}{M_{W_R}}\right)^2 \left(\frac{g_r}{g_l}\right)^2 \sum_{i=1,2,3} V_{ei}^{\nu\nu} V_{ei}^{N\nu} \frac{1}{|p|} \\
 \mathcal{A}_\lambda^N &\propto G_F^2 \left(\frac{M_{W_L}}{M_{W_R}}\right)^2 \left(\frac{g_r}{g_l}\right)^2 \sum_{j=1,2,3} V_{ej}^{\nu N} V_{ej}^{NN} \frac{|p|}{M_{N_j}^2} \\
 \mathcal{A}_\lambda^S &\propto G_F^2 \left(\frac{M_{W_L}}{M_{W_R}}\right)^2 \left(\frac{g_r}{g_l}\right)^2 \sum_{k=1,2,3} V_{ek}^{\nu\nu} V_{ek}^{NS} \frac{|p|}{M_{S_k}^2}
 \end{aligned} \tag{A5}$$

2 Feynman amplitudes for η -mechanism

$$\begin{aligned}
\mathcal{A}_\lambda^\nu &\propto G_F^2 \left(\frac{g_r}{g_l}\right) \text{ten}\zeta \sum_{i=1,2,3} V_{ei}^{\nu\nu} V_{ei}^{N\nu} \frac{1}{|p|} \\
\mathcal{A}_\lambda^N &\propto G_F^2 \left(\frac{g_r}{g_l}\right) \text{ten}\zeta \sum_{j=1,2,3} V_{ej}^{\nu N} V_{ej}^{NN} \frac{|p|}{M_{N_j}^2} \\
\mathcal{A}_\lambda^S &\propto G_F^2 \left(\frac{g_r}{g_l}\right) \text{ten}\zeta \sum_{k=1,2,3} V_{ek}^{\nu S} V_{ek}^{NS} \frac{|p|}{M_{S_k}^2}
\end{aligned} \tag{A6}$$

d. Contribution due to doubly charged Higgs boson

The Feynman amplitude and diagram due to doubly charged Higgs boson are given in equation A7 and in Figure 15 respectively

$$\begin{aligned}
\mathcal{A}_{LL}^{\Delta_L} &\propto G_F^2 \sum_{i=1,2,3} \frac{1}{M_{\Delta_L}^2} V_{ei}^{\nu\nu^2} m_{\nu_i} \\
\mathcal{A}_{RR}^{\Delta_R} &\propto G_F^2 \sum_{i=1,2,3} \left(\frac{M_{W_L}}{M_{W_R}}\right)^4 \left(\frac{g_r}{g_l}\right)^4 \frac{1}{M_{\Delta_R}^2} V_{ei}^{NN^2} M_{N_i}
\end{aligned} \tag{A7}$$

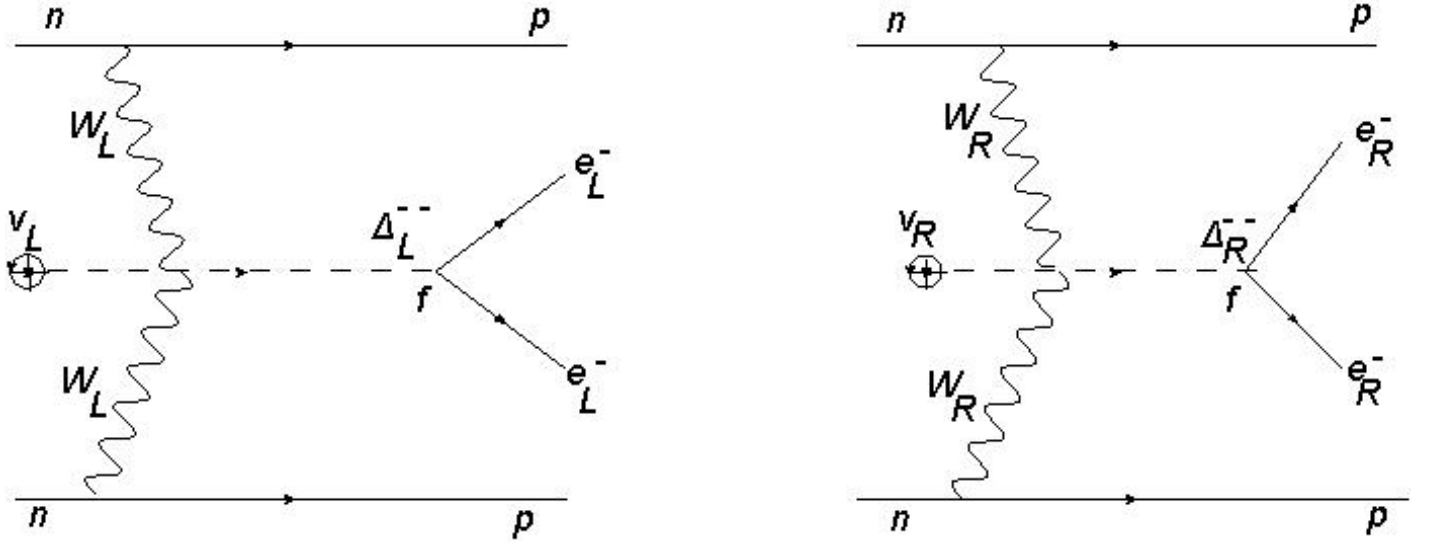


FIG. 15: Feynman diagram for doubly charged Higgs boson

Appendix B: Half-life of $0\nu\beta\beta$ decay

The analytic expression for the inverse half life of neutrino less double beta decay considering all the contribution can be written in the following way [61, 62]

$$[T_{1/2}^\nu]^{-1} = G_{01}^{0\nu} |M_\nu^{0\nu}|^2 |\eta_{LL}^\nu|^2 + |M_N^{0\nu}|^2 |\eta_{LL}^{N,S}|^2 + |M_\nu^{0\nu}|^2 |\eta_{RR}^\nu|^2 + |M_N^{0\nu}|^2 |\eta_{RR}^{N,S}|^2 + |M_\lambda^{0\nu} \eta_\lambda + M_\eta^{0\nu} \eta_\eta|^2. \tag{B1}$$

Where $G_{01}^{0\nu}$ is the phase space factor and $M_i^{0\nu}$ ($i = \nu, N, \lambda, \eta$) is the nuclear matrix elements and $|\eta|$ is a dimensionless parameter. The experimental values of nuclear mass matrix for the isotope Ge and Xe is given in the Table IX. Considering only the standard contribution due to the exchange of light Majorana neutrino we can write inverse half life formula in the following way [56]

$$[T_{1/2}^\nu]^{-1} = G_{01}^{0\nu} |M_\nu^{0\nu}|^2 |\eta_{LL}^\nu|^2 \quad (\text{B2})$$

and by using equation (A2), one can modify equation (B2) in terms of effective mass $|m_{ee,L}^\nu|$

$$[T_{1/2}^\nu]^{-1} = G_{01}^{0\nu} \left| \frac{M_\nu^{0\nu}}{m_e} \right|^2 |m_{ee,L}^\nu|^2 \quad (\text{B3})$$

where, m_e is mass of the electron. One can take the term $\mathcal{K}_{0\nu} = G_{01}^{0\nu} \left| \frac{M_\nu^{0\nu}}{m_e} \right|^2$ as a normalizing factor for other contribution and can write equation (B1) in terms of the effective Majorana mass parameter in the following way

Isotope	$G_{01}^{0\nu}$	$M_\nu^{0\nu}$	$M_N^{0\nu}$	$M_\lambda^{0\nu}$	$M_\eta^{0\nu}$
76_{Ge}	5.77×10^{-15}	2.58 – 6.64	233 – 412	1.75 – 3.76	235 – 637
136_{Xe}	3.56×10^{-14}	1.57 – 3.85	164 – 172	1.92 – 2.49	370 – 419

TABLE IX: Allowed ranges of phase space factors and nuclear matrix elements

$$[T_{1/2}^{0\nu}]^{-1} = \mathcal{K}_{0\nu} \left[|m_{ee,L}^\nu|^2 + |m_{ee,L}^S + m_{ee,L}^N|^2 + |m_{ee,R}^\nu + m_{ee,R}^S + m_{ee,R}^N|^2 + |m_{ee,\lambda}^\nu + m_{ee,\lambda}^S + m_{ee,\lambda}^N|^2 + |m_{ee,\eta}^\nu + m_{ee,\eta}^S + m_{ee,\eta}^N|^2 \right] \quad (\text{B4})$$

Appendix C: A_4 group

A_4 is a group which represents even permutation of four objects. It has a total of 12 elements and have two generator, represented by S and T . A_4 has 4 conjugacy class which means that A_4 has four irreducible representation. Among those four irreducible representation, three are one dimensional ($1, 1', 1''$) and one is three dimensional. The product rules of two triplet (ψ_1, ψ_2, ψ_3) and (ϕ_1, ϕ_2, ϕ_3) in the T diagonal basis are given bellow

$$\begin{aligned} \begin{pmatrix} \psi_1 \\ \psi_2 \\ \psi_3 \end{pmatrix} \times \begin{pmatrix} \phi_1 \\ \phi_2 \\ \phi_3 \end{pmatrix} &= \left(\psi_1\phi_1 + \psi_2\phi_3 + \psi_3\phi_2 \right) + \left(\psi_3\phi_3 + \psi_1\phi_2 + \psi_2\phi_1 \right) + \left(\psi_2\phi_2 + \psi_3\phi_1 + \psi_1\phi_3 \right) \\ &+ \begin{pmatrix} 2\psi_1\phi_1 - \psi_2\phi_3 - \psi_3\phi_2 \\ 2\psi_3\phi_3 - \psi_1\phi_2 - \psi_2\phi_1 \\ 2\psi_2\phi_2 - \psi_1\phi_3 - \psi_3\phi_1 \end{pmatrix} + \begin{pmatrix} \psi_2\phi_3 - \psi_3\phi_2 \\ \psi_1\phi_2 - \psi_2\phi_1 \\ \psi_3\phi_1 - \psi_1\phi_3 \end{pmatrix} . \end{aligned}$$

The multiplication rules are given bellow

$$3 \times 3 = 1 + 1' + 1'' + 3 + 3.$$

$$1' \times 1' = 1'', \quad 1' \times 1'' = 1, \quad 1'' \times 1'' = 1'.$$

- [1] S. Fukuda et al. Constraints on neutrino oscillations using 1258 days of Super-Kamiokande solar neutrino data. *Phys. Rev. Lett.*, 86:5656–5660, 2001.
- [2] Q. R. Ahmad et al. Measurement of day and night neutrino energy spectra at SNO and constraints on neutrino mixing parameters. *Phys. Rev. Lett.*, 89:011302, 2002.
- [3] Q. R. Ahmad et al. Direct evidence for neutrino flavor transformation from neutral current interactions in the Sudbury Neutrino Observatory. *Phys. Rev. Lett.*, 89:011301, 2002.
- [4] Abhijit Bandyopadhyay, Sandhya Choubey, Srubabati Goswami, and Kamales Kar. Impact of the first SNO results on neutrino mass and mixing. *Phys. Lett. B*, 519:83–92, 2001.
- [5] Justin Evans. The MINOS Experiment: Results and Prospects. *Adv. High Energy Phys.*, 2013:182537, 2013.
- [6] F. P. An et al. Observation of electron-antineutrino disappearance at Daya Bay. *Phys. Rev. Lett.*, 108:171803, 2012.
- [7] K. Abe et al. Indication of Electron Neutrino Appearance from an Accelerator-produced Off-axis Muon Neutrino Beam. *Phys. Rev. Lett.*, 107:041801, 2011.
- [8] Thierry Lasserre, Guillaume Mention, Michel Cribier, Antoine Collin, Vincent Durand, Vincent Fischer, Jonathan Gaffiot, David Lhuillier, Alain Letourneau, and Matthieu Vivier. Comment on Phys. Rev. Lett. 108, 191802 (2012): 'Observation of Reactor Electron Antineutrino Disappearance in the RENO Experiment'. 5 2012.
- [9] N. Aghanim et al. Planck 2018 results. VI. Cosmological parameters. *Astron. Astrophys.*, 641:A6, 2020. [Erratum: *Astron. Astrophys.* 652, C4 (2021)].
- [10] X. Qian and P. Vogel. Neutrino Mass Hierarchy. *Prog. Part. Nucl. Phys.*, 83:1–30, 2015.
- [11] Anushree Ghosh, Tarak Thakore, and Sandhya Choubey. Determining the Neutrino Mass Hierarchy with INO, T2K, NOvA and Reactor Experiments. *JHEP*, 04:009, 2013.
- [12] G. Barenboim, John F. Beacom, L. Borisso, and Boris Kayser. CPT Violation and the Nature of Neutrinos. *Phys. Lett. B*, 537:227–232, 2002.
- [13] M. Czakon, J. Gluza, and M. Zralek. Nature of neutrinos in the light of present and future experiments. *Phys. Lett. B*, 465:211–218, 1999.

- [14] Rabindra N. Mohapatra and Goran Senjanovic. Neutrino Mass and Spontaneous Parity Nonconservation. *Phys. Rev. Lett.*, 44:912, 1980.
- [15] Murray Gell-Mann, Pierre Ramond, and Richard Slansky. Complex Spinors and Unified Theories. *Conf. Proc. C*, 790927:315–321, 1979.
- [16] J. Schechter and J. W. F. Valle. Neutrino Masses in $SU(2) \times U(1)$ Theories. *Phys. Rev. D*, 22:2227, 1980.
- [17] T. P. Cheng and Ling-Fong Li. Neutrino Masses, Mixings and Oscillations in $SU(2) \times U(1)$ Models of Electroweak Interactions. *Phys. Rev. D*, 22:2860, 1980.
- [18] C. Wetterich. Neutrino Masses and the Scale of B-L Violation. *Nucl. Phys. B*, 187:343–375, 1981.
- [19] M. Magg and C. Wetterich. Neutrino Mass Problem and Gauge Hierarchy. *Phys. Lett. B*, 94:61–64, 1980.
- [20] Robert Foot, H. Lew, X. G. He, and Girish C. Joshi. Seesaw Neutrino Masses Induced by a Triplet of Leptons. *Z. Phys. C*, 44:441, 1989.
- [21] Jogesh C. Pati and Abdus Salam. Lepton Number as the Fourth Color. *Phys. Rev. D*, 10:275–289, 1974. [Erratum: *Phys.Rev.D* 11, 703–703 (1975)].
- [22] G. Senjanovic and Rabindra N. Mohapatra. Exact Left-Right Symmetry and Spontaneous Violation of Parity. *Phys. Rev. D*, 12:1502, 1975.
- [23] N. G. Deshpande, J. F. Gunion, Boris Kayser, and Fredrick I. Olness. Left-right symmetric electroweak models with triplet Higgs. *Phys. Rev. D*, 44:837–858, 1991.
- [24] R. N. Mohapatra and Jogesh C. Pati. A Natural Left-Right Symmetry. *Phys. Rev. D*, 11:2558, 1975.
- [25] H. Georgi and S. L. Glashow. Unity of All Elementary Particle Forces. *Phys. Rev. Lett.*, 32:438–441, 1974.
- [26] Thomas G. Rizzo and Goran Senjanovic. Grand Unification and Parity Restoration at Low-Energies. 1. Phenomenology. *Phys. Rev. D*, 24:704, 1981. [Erratum: *Phys.Rev.D* 25, 1447 (1982)].
- [27] D. Chang, R. N. Mohapatra, and M. K. Parida. Decoupling Parity and $SU(2)$ -R Breaking Scales: A New Approach to Left-Right Symmetric Models. *Phys. Rev. Lett.*, 52:1072, 1984.
- [28] Stephen F. King and Christoph Luhn. Neutrino Mass and Mixing with Discrete Symmetry. *Rept. Prog. Phys.*, 76:056201, 2013.
- [29] Guido Altarelli and Ferruccio Feruglio. Discrete Flavor Symmetries and Models of Neutrino Mixing. *Rev. Mod. Phys.*, 82:2701–2729, 2010.
- [30] Ernest Ma and G. Rajasekaran. Softly broken $A(4)$ symmetry for nearly degenerate neutrino masses. *Phys. Rev. D*, 64:113012, 2001.
- [31] Guido Altarelli, Ferruccio Feruglio, and Luca Merlo. Revisiting Bimaximal Neutrino Mixing in a Model with $S(4)$ Discrete Symmetry. *JHEP*, 05:020, 2009.
- [32] P. P. Novichkov, J. T. Penedo, S. T. Petcov, and A. V. Titov. Generalised CP Symmetry in Modular-Invariant Models of Flavour. *JHEP*, 07:165, 2019.

- [33] Simon J. D. King and Stephen F. King. Fermion mass hierarchies from modular symmetry. *JHEP*, 09:043, 2020.
- [34] Mitesh Kumar Behera, Shivaramakrishna Singirala, Subhasmita Mishra, and Rukmani Mohanta. A modular A_4 symmetric scotogenic model for neutrino mass and dark matter. *J. Phys. G*, 49(3):035002, 2022.
- [35] Mitesh Kumar Behera, Subhasmita Mishra, Shivaramakrishna Singirala, and Rukmani Mohanta. Implications of A_4 modular symmetry on neutrino mass, mixing and leptogenesis with linear seesaw. *Phys. Dark Univ.*, 36:101027, 2022.
- [36] Takaaki Nomura, Hiroshi Okada, and Sudhanwa Patra. An inverse seesaw model with A_4 -modular symmetry. *Nucl. Phys. B*, 967:115395, 2021.
- [37] Jotin Gogoi, Nayana Gautam, and Mrinal Kumar Das. Neutrino masses and mixing in minimal inverse seesaw using A_4 modular symmetry. *Int. J. Mod. Phys. A*, 38(03):2350022, 2023.
- [38] Ankita Kakoti, Bichitra Bijay Boruah, and Mrinal Kumar Das. Minimal left–right symmetric model with A_4 modular symmetry. *Int. J. Mod. Phys. A*, 38(28):2350150, 2023.
- [39] Ranjeet Kumar, Priya Mishra, Mitesh Kumar Behera, Rukmani Mohanta, and Rahul Srivastava. Predictions from scoto-seesaw with A_4 modular symmetry. *Phys. Lett. B*, 853:138635, 2024.
- [40] Hiroshi Okada and Yuta Orikasa. Neutrino mass model with a modular S_4 symmetry. 8 2019.
- [41] P. P. Novichkov, J. T. Penedo, and S. T. Petcov. Double cover of modular S_4 for flavour model building. *Nucl. Phys. B*, 963:115301, 2021.
- [42] P. P. Novichkov, J. T. Penedo, S. T. Petcov, and A. V. Titov. Modular A_5 symmetry for flavour model building. *JHEP*, 04:174, 2019.
- [43] D. Chang, R. N. Mohapatra, and M. K. Parida. A New Approach to Left-Right Symmetry Breaking in Unified Gauge Theories. *Phys. Rev. D*, 30:1052, 1984.
- [44] M. Sruthilaya, Rukmani Mohanta, and Sudhanwa Patra. Neutrino mass and neutrinoless double beta decay in $SO(10)$ GUT with Pati–Salam symmetry. *J. Phys. G*, 45(7):075004, 2018.
- [45] Francisco J. de Anda and Stephen F. King. Modular flavour symmetry and orbifolds. *JHEP*, 06:122, 2023.
- [46] Reinier de Adelhart Toorop, Ferruccio Feruglio, and Claudia Hagedorn. Finite Modular Groups and Lepton Mixing. *Nucl. Phys. B*, 858:437–467, 2012.
- [47] S. Ferrara, . D. Lust, and S. Theisen. Target Space Modular Invariance and Low-Energy Couplings in Orbifold Compactifications. *Phys. Lett. B*, 233:147–152, 1989.
- [48] Ferruccio Feruglio. *Are neutrino masses modular forms?*, pages 227–266. 2019.
- [49] Supriya Senapati, Sudhanwa Patra, Prativa Pritimita, and Chayan Majumdar. A comparative study of $0\nu\beta\beta$ decay in symmetric and asymmetric left-right model. *Nucl. Phys. B*, 954:115000, 2020.
- [50] Ram Lal Awasthi, M. K. Parida, and Sudhanwa Patra. Neutrino masses, dominant neutrinoless double beta decay, and observable lepton flavor violation in left-right models and $SO(10)$ grand unification with

- low mass W_R, Z_R bosons. *JHEP*, 08:122, 2013.
- [51] M. K. Parida and Sudhanwa Patra. Left-right models with light neutrino mass prediction and dominant neutrinoless double beta decay rate. *Phys. Lett. B*, 718:1407–1412, 2013.
- [52] W. Grimus and L. Lavoura. The Seesaw mechanism at arbitrary order: Disentangling the small scale from the large scale. *JHEP*, 11:042, 2000.
- [53] P. S. Bhupal Dev and R. N. Mohapatra. TeV Scale Inverse Seesaw in SO(10) and Leptonic Non-Unitarity Effects. *Phys. Rev. D*, 81:013001, 2010.
- [54] Ram Lal Awasthi and Mina K. Parida. Inverse Seesaw Mechanism in Nonsupersymmetric SO(10), Proton Lifetime, Nonunitarity Effects, and a Low-mass Z' Boson. *Phys. Rev. D*, 86:093004, 2012.
- [55] Nuno Rosa Agostinho, G. C. Branco, Pedro M. F. Pereira, M. N. Rebelo, and J. I. Silva-Marcos. Can one have significant deviations from leptonic 3×3 unitarity in the framework of type I seesaw mechanism? *Eur. Phys. J. C*, 78(11):895, 2018.
- [56] Prativa Pritimita, Nitali Dash, and Sudhanwa Patra. Neutrinoless Double Beta Decay in LRSM with Natural Type-II seesaw Dominance. *JHEP*, 10:147, 2016.
- [57] Alberto Garfagnini. Latest results from GERDA Phase II experiment on ^{76}Ge double-beta decay and exotic decay searches. *PoS*, EPS-HEP2023:158, 2024.
- [58] G. Anton et al. Search for Neutrinoless Double- β Decay with the Complete EXO-200 Dataset. *Phys. Rev. Lett.*, 123(16):161802, 2019.
- [59] S. Abe et al. Search for the Majorana Nature of Neutrinos in the Inverted Mass Ordering Region with KamLAND-Zen. *Phys. Rev. Lett.*, 130(5):051801, 2023.
- [60] A. Gando et al. Limit on Neutrinoless $\beta\beta$ Decay of ^{136}Xe from the First Phase of KamLAND-Zen and Comparison with the Positive Claim in ^{76}Ge . *Phys. Rev. Lett.*, 110(6):062502, 2013.
- [61] James Barry and Werner Rodejohann. Lepton number and flavour violation in TeV-scale left-right symmetric theories with large left-right mixing. *JHEP*, 09:153, 2013.
- [62] K. Muto, E. Bender, and H. V. Klapdor. Nuclear Structure Effects on the Neutrinoless Double Beta Decay. *Z. Phys. A*, 334:187–194, 1989.